A Molecular Mechanics AMBER-Type Force Field for Modeling Platinum Complexes of Guanine Derivatives

Shijie Yao, John P. Plastaras, and Luigi G. Marzilli*

Department of Chemistry and Cherry L. Emerson Center for Scientific Computation, Emory University, Atlanta, Georgia 30322

Received June 16, 1994[⊗]

A force field, developed and designated here as DNA/Pt, was optimized for modeling Pt ammine/amine complexes of guanine derivatives (G) bound via N7. DNA/Pt was based on the all-atom type force field of Weiner et al. (Weiner, S. J.; Kollman, P. A.; Nguyen, D. T.; Case, D. A. *J. Comput. Chem.* **1986**, *7*, 230) as modified by Veal and Wilson (Veal, J. M.; Wilson, D. W. *J. Biomol. Struct. Dyn.* **1991**, *8*, 1119). New atom types were created for Pt, N7 of G, and the amine/ammine N and H atoms. Force field parameters for these new atom types were developed by comparing force field parameters found in the literature with the structural features of published crystal structures. Pt out-of-plane bending was treated by a single improper torsion barrier, C8−N7−C5−Pt. The force constant parameter for the improper torsional deformation barrier was determined in this study by fitting the resulting out-of-plane bending potential curve onto the corresponding profile from *ab initio* calculations on $[Pt(NH_3)_3(Ade)]^{2+}$ (Kozelka, J.; Savinelli, R.; Berthier, G.; Flament, J.-P.; Lavery, R. *J. Comput. Chem.* **1993**, *14*, 45). The DNA/Pt force field also includes parameters for the van der Waals radius of the Pt atom and for O6−HN(amine/ammine) H-bonding. An empirical charge distribution method was used to modify the atomic point charges on the *cis*-$[PtA_2G_2]$ moiety, where A = amine or $^1/_2$ of a diamine. In general, widely used procedures were adopted. For example, a distance-dependent dielectric constant of $\epsilon = 4r_{ij}$ and partially neutralized phosphates were used to represent solvent and counterion. The validity of this new DNA/Pt force field was evaluated by a number of test cases. Conformational features determined by either X-ray crystallographic or NMR techniques were reproduced well by the calculations. The rotational barriers for a number of complexes were calculated and were found to agree with NMR data quite well. The calculated relative stabilities of head-to-head and head-to-tail conformers of some complexes are also in good agreement with experimental results. Finally, an initial attempt to model lattice effects was found to improve the fit between calculated and crystal structures of the *cis*-$[PtA_2G_2]$ species.

Introduction

A large number of Pt(II)/Pt(IV) complexes have been found to have anticancer activity.[1] There currently exist several classes of Pt anticancer drugs, but we restrict discussion to the widely approved and clinically used *cis*-PtA_2X_2 class (where A = amine/ammine or $^1/_2$ diamine and X = anion or $^1/_2$ dianion). It is now widely accepted that DNA is the major cellular target of these active *cis*-PtA_2X_2 complexes.[2,3] Pt binds to DNA, preferentially to the N7 position of guanine residues,[4−6] [G will be used to represent any derivative of guanine, but specific derivatives may be identified here, e.g. 9-ethylguanine as 9-EtGua]. There is also a wealth of evidence that the *cis* ammines or amines in the Pt complexes affect anticancer activity.[3,7,8] The major DNA−*cis*-PtA_2 adduct formed, both *in vitro* and *in vivo*, is the intrastrand G*pG* chelate.[4−6,9,10] For oligonucleotides, G's platinated at N7 are designated as G*. Since platination of DNA can interrupt the substrate recognition for nucleases and polymerases[11,12] and alter other structural properties of DNA,[13,14] substantial changes in DNA structure have been suggested.

As mentioned above, our focus is on *cis*-PtA_2X_2 drugs, and we have concentrated our modeling efforts on these drugs. However, since other types of Pt drugs may function by binding to DNA,[1,15−17] our results may have relevance to these as well. The structural features of DNA−*cis*-PtA_2 complexes have been most extensively studied. The available crystal structures of nucleobase−*cis*-PtA_2, nucleoside/nucleotide−*cis*-PtA_2, and short DNA single strand−*cis*-PtA_2 complexes have provided valuable insights into the ways in which Pt(II) complexes bind to DNA constituents.[18] High resolution NMR studies have also yielded a wealth of structural information on nucleotide−*cis*-PtA_2,[19,20] short single strand oligonucleotide−*cis*-PtA_2,[21] and DNA duplex

[⊗] Abstract published in *Advance ACS Abstracts,* December 1, 1994.

(1) Farrell, N. *Metal Complexes as Drugs and Chemotherapeutic Agents*; Kluwer Academic: Dordrecht, The Netherlands, 1989.
(2) Sherman, S. E.; Lippard, S. J. *Chem. Rev.* **1987**, *87*, 1153.
(3) Reedijk, J.; Fichtinger-Schepman, A. M. J.; van Oosterom, A. T.; van de Putte, P. *Struct. Bonding (Berlin)* **1987**, *67*, 53.
(4) Fichtinger-Schepman, A. M. J.; van der Veer, J. L.; den Hartog, J. H. J.; Lohman, P. H. M.; Reedijk, J. *Biochemistry* **1985**, *24*, 707.
(5) Fichtinger-Schepman, A. M. J.; van Oosterom, A. T.; Lohman, P. H. M.; Berends, F. *Cancer Res.* **1987**, *47*, 3000.
(6) Eastman, A. *Biochemistry* **1986**, *25*, 3912.
(7) Johnson, N. P.; Butour, J.-L.; Villani, G.; Wimmer, F. L.; Defais, M.; Pierson, V.; Brabec, V. *Prog. Clin. Biochem. Med.* **1989**, *10*, 1.
(8) Leh, F. K. V.; Wolf, W. *J. Pharm. Sci.* **1976**, *65*, 315.
(9) Pinto, A. L.; Lippard, S. J. *Biochim. Biophys. Acta* **1985**, *780*, 167.
(10) Laoui, A.; Kozelka, J.; Chottard, J.-C. *Inorg. Chem.* **1988**, *27*, 2751.
(11) Pinto, A. L.; Lippard, S. J. *Proc. Natl. Acad. Sci. U.S.A.* **1985**, *82*, 4616.
(12) Ushay, H. M.; Tullius, T. D.; Lippard, S. J. *Biochemistry* **1981**, *20*, 3744.
(13) Cohen, G. L.; Bauer, W. R.; Barton, J. K.; Lippard, S. J. *Science (Washington, D.C.)* **1979**, *203*, 1014.
(14) Macquet, J.-P.; Butour, J.-L. *Biochimie* **1978**, *60*, 901.
(15) Farrell, N.; Kelland, L. R.; Roberts, J. D.; Van Beuischem, M. *Cancer Res.* **1992**, *52*, 5065.
(16) Farrell, N. *Comments Inorg. Chem.* **1994**, in press.
(17) Hollis, L. S. In *Platinum and Other Metal Coordination Compounds in Cancer Chemotherapy*; Howell, S. B., Ed.; Plenum Press: New York, 1991; pp 115−125.
(18) Lippert, B. *Prog. Inorg. Chem.* **1989**, *37*, 1.
(19) Reily, M. D.; Marzilli, L. G. *J. Am. Chem. Soc.* **1986**, *108*, 6785.
(20) Xu, Y.; Natile, G.; Intini, F. P.; Marzilli, L. G. *J. Am. Chem. Soc.* **1990**, *112*, 8177.

0020-1669/94/1333-6061$04.50/0

oligonucleotide−*cis*-PtA_2 complexes.[22−28] However, a clear detailed definition of the structure of *cis*-PtA_2 DNA duplex adducts has still not been reported, and there are reasons to believe that many types of such adducts could form depending on sequence.[28] Furthermore, evidence exists that such adducts may exhibit dynamic properties, and molecular dynamics/molecular mechanics simulation will be needed to help understand this conformational flexibility.

We are interested in obtaining more detailed structural information about *cis*-PtA_2−DNA interactions by both experimental (high-resolution 2D NMR) and computational (molecular mechanics and dynamics) techniques. Considerable informative computational effort has been expended on nucleic acids and their complexes with organic compounds,[29−32] but relatively little such theoretical effort has been reported for DNA−metal complexes due to the difficulties in the parametrization of force field parameters related to metal atoms. Some molecular mechanics calculations on *cis*-PtA_2 DNA complexes have been explored with some success,[26,33−40] but a thoroughly developed force field for DNA−Pt modeling remains to be presented.

The AMBER force field was developed by Weiner et al.[41] for modeling nucleic acids and is widely used in the DNA/RNA field; it is integrated into most commercial software packages. The AMBER force field has also been used to model metal complexes.[42] Therefore, we selected AMBER for the development of a suitable force field to model DNA−*cis*-PtA_2 adducts.

Methods

All modeling studies employed the Discover 2.9 software in the Insight 2.2.0 modeling package (Biosym Technologies, San Diego, CA). Calculations were done either on a Silicon Graphics Indigo workstation or IBM RISC System/6000 computer. Standard AMBER strain energies described in eq 1 were used for all energy calculations. We

$$E_{\text{total}} = E_{\text{bond stretch}} + E_{\text{angle bend}} + E_{\text{torsional}} + E_{\text{van der Waals}} + E_{\text{electrostatic}} + E_{\text{hydrogen bonding}} + E_{\text{improper}} = \sum K_r(r-r_0)^2 + \sum K_\theta(\theta-\theta_0)^2 + \sum V_n[1 + \cos(n\phi - \phi_0)] + \sum \epsilon_{ij}{}^*[(R_{ij}/r_{ij})^{12} - 2(R_{ij}/r_{ij})^6] + \sum (q_i q_j)/\epsilon r_{ij} + \sum [A_{ij}/r_{ij}{}^{12} - B_{ij}/r_{ij}{}^{10}] + \sum K_\chi[1 + \cos(n\chi + \chi_0)] \quad (1)$$

adopted the recent changes made to the AMBER force field because the changes generally improved DNA/RNA modeling.[43] We implemented our force field based on the distance-dependent dielectric constant of $\epsilon = 4r_{ij}$ and partially neutralized phosphates, a combination that has been commonly employed in DNA/RNA modeling.[44−48]

To select the equilibrium values needed for the force field and to assess the ranges of bending and torsional angles, we first analyzed available crystallographic information on relevant Pt complexes. Coordinates of three classes of G structures were retrieved from the Cambridge Structural Database[49] (through 1992): (i) no extraannular substituent at N7 (**free**); (ii) H at N7 (**protonated**); (iii) Pt at N7 (**platinated**). References[49−61] for the **platinated** data sets are listed in Table 1. The structures were displayed and the geometric parameters were measured with Insight 2.2.0. Crystal structure reliability for small unrestrained structures was evaluated with the interior angles of the five-membered guanine rings as a criterion. All data points from structure J (Table 1) were discarded due to large deviations from the calculated averages of the five interior angles. The **free** and **protonated** data sets were similarly filtered, and the average values of the interior angles for all three data sets are available in the supplementary material (Table S1).

In order to describe the square planar geometry of four coordinate Pt complexes (i.e., to describe the right angle and the coaxial relationships between the *cis* and the *trans* bonds, respectively), six new atom types were introduced in the new DNA/Pt force field (Table 2 and Figure 1). PT is a suitable atom type for the unique Pt atom. Atom type NB1 and/or NB2 is assigned to the N7 atom of the Pt−N7 bound guanine base. Atom type N31 and/or N32 is assigned to the metal-bound nitrogen atoms in the amine ligands. The H3 atom type is assigned to the hydrogens bound to N31 or N32 nitrogens.

(21) Fouts, C. S.; Marzilli, L. G.; Byrd, R. A.; Summers, M. F.; Zon, G.; Shinozuka, K. *Inorg. Chem.* **1988**, *27*, 366.
(22) den Hartog, J. H. J.; Altona, C.; van Boom, J. H.; Reedijk, J. *FEBS Lett.* **1984**, *176*, 393.
(23) den Hartog, J. H. J.; Altona, C.; van Boom, J. H.; van der Marel, G. A.; Haasnoot, C. A. G.; Reedijk, J. *J. Am. Chem. Soc.* **1984**, *106*, 1528.
(24) den Hartog, J. H. J.; Altona, C.; van Boom, J. H.; van der Marel, G. A.; Haasnoot, C. A. G.; Reedijk, J. *J. Biomol. Struct. Dyn.* **1985**, *2*, 1137.
(25) Van Hemelryck, B.; Guittet, E.; Chottard, G.; Girault, J.-P.; Huynh-Dinh, T.; Lallemand, J.-Y.; Igolen, J.; Chottard, J.-C. *J. Am. Chem. Soc.* **1984**, *106*, 3037.
(26) Herman, F.; Kozelka, J.; Stoven, V.; Guittet, E.; Girault, J.-P.; Huynh-Dinh, T.; Igolen, J.; Lallemand, J.-Y.; Chottard, J.-C. *Eur. J. Biochem.* **1990**, *194*, 119.
(27) Xu, Y. Ph.D. Thesis, Emory University, 1992.
(28) Iwamoto, M.; Mukundan, S., Jr.; Marzilli, L. G. *J. Am. Chem. Soc.* **1994**, *116*, 6238−6244.
(29) Yao, S.; Wilson, W. D. *J. Biomol. Struct. Dyn.* **1992**, *10*, 367.
(30) Pullman, B. *Molecular Basis of Specificity in Nucleic Acid-Drug Interactions, The Jerusalem Symposia on Quantum Chemistry and Biochemistry Vol. 23*; Kluwer Academic: Boston, MA, 1990; pp 401−422.
(31) Caldwell, J.; Kollman, P. A. *Biopolymers* **1986**, *25*, 246.
(32) Lybrand, T.; Kollman, P. A. *Biopolymers* **1985**, *24*, 1863.
(33) Reily, M. D.; Hambley, T. W.; Marzilli, L. G. *J. Am. Chem. Soc.* **1988**, *110*, 2999.
(34) Kozelka, J.; Petsko, G. A.; Lippard, S. J.; Quigley, G. J. *J. Am. Chem. Soc.* **1985**, *107*, 4079.
(35) Kozelka, J.; Archer, S.; Petsko, G. A.; Lippard, S. J.; Quigley, G. J. *Biopolymers* **1987**, *26*, 1245.
(36) Kozelka, J.; Chottard, J.-C. *Biophys. Chem.* **1990**, *35*, 165.
(37) Kozelka, J.; Petsko, G. A.; Quigley, G. J.; Lippard, S. J. *Inorg. Chem.* **1986**, *25*, 1075.
(38) Hambley, T. W. *Inorg. Chem.* **1988**, *27*, 1073.
(39) Hambley, T. W. *Inorg. Chem.* **1991**, *30*, 937.
(40) Hay, B. P. *Coord. Chem. Rev.* **1993**, *126*, 177.
(41) Weiner, S. J.; Kollman, P. A.; Nguyen, D. T.; Case, D. A. *J. Comput. Chem.* **1986**, *7*, 230.
(42) Hansen, L.; Cini, R.; Taylor, A., Jr.; Marzilli, L. G. *Inorg. Chem.* **1992**, *31*, 2801.
(43) Veal, J. M.; Wilson, W. D. *J. Biomol. Struct. Dyn.* **1991**, *8*, 1119.
(44) Hartmann, B.; Lavery, R. *J. Biomol. Struct. Dyn.* **1989**, *7*, 363.
(45) Hingerty, B. E.; Figueroa, S.; Hayden, T. L.; Broyde, S. *Biopolymers* **1989**, *28*, 1192.
(46) Mao, M. H.; Olson, W. K. *J. Biomol. Struct. Dyn.* **1989**, *7*, 661.
(47) Orozco, M.; Laughton, C. A.; Herzyk, P.; Neidle, S. *J. Biomol. Struct. Dyn.* **1990**, *8*, 359.
(48) Srinivasan, A. R.; Olson, W. K. *J. Biomol. Struct. Dyn.* **1987**, *4*, 895.
(49) Allen, F. H.; Davies, J. E.; Galloy, J. J.; Johnson, O.; Kennard, O.; Macrae, C. F.; Mitchell, E. M.; Mitchell, G. F.; Smith, J. M.; Watson, D. G. *J. Chem. Inf. Comput. Sci.* **1991**, *31*, 187.
(50) Admiraal, G.; van der Veer, J. L.; de Graff, R. A. G.; den Hartog, J. H. J.; Reedijk, J. *J. Am. Chem. Soc.* **1987**, *109*, 592.
(51) Schöllhorn, H.; Raudaschl-Sieber, G.; Müller, G.; Thewalt, U.; Lippert, B. *J. Am. Chem. Soc.* **1985**, *107*, 5932.
(52) Sherman, S. E.; Gibson, D.; Wang, A. H.-J.; Lippard, S. J. *J. Am. Chem. Soc.* **1988**, *110*, 7368.
(53) Lippert, B.; Raudaschl, G.; Lock, C. J. L.; Pilon, P. *Inorg. Chim. Acta* **1984**, *93*, 43.
(54) Cramer, R. E.; Dahlstrom, P. L.; Seu, M. J. T.; Norton, T.; Kashiwagi, M. *Inorg. Chem.* **1980**, *19*, 148.
(55) Sindellari, L.; Schöllhorn, H.; Thewalt, U.; Raudaschl-Sieber, G.; Lippert, B. *Inorg. Chim. Acta* **1990**, *168*, 27.
(56) Orbell, J. D.; Solorzano, C.; Marzilli, L. G.; Kistenmacher, T. J. *Inorg. Chem.* **1982**, *21*, 3806.
(57) Faggiani, R.; Lippert, B.; Lock, C. J. L.; Speranzini, R. A. *Inorg. Chem.* **1982**, *21*, 3216.
(58) Melanson, R.; Rochon, F. D. *Can. J. Chem.* **1979**, *57*, 57.
(59) Marzilli, L. G.; Chalilpoyil, P.; Chiang, C. C.; Kistenmacher, T. J. *J. Am. Chem. Soc.* **1980**, *102*, 2480.
(60) Orbell, J. D.; Taylor, M. R.; Birch, S. L.; Lawton, S. E.; Vilkins, L. M.; Keefe, L. J. *Inorg. Chim. Acta* **1988**, *152*, 125.
(61) Coll, M.; Sherman, S. E.; Gibson, D.; Lippard, S. J.; Wang, A. H.-J. *J. Biomol. Struct. Dyn.* **1990**, *8*, 315.

Table 1. Cambridge Structural Database and Short Codes for Pt Complexes of G Derivatives

short code	CSD code[a]	formula	ref
A	FEDFID[b]	*cis*-[Pt(NH_3)$_2$d(C_1pG_2*pG_3*)]·H_2O	50
B	DEGXAO	*cis*-[Pt(NH_3)$_2$(9-EtGua)$_2$]SO_4·$4H_2O$	51
C	DETLIX11[c]	*cis*-[Pt(NH_3)$_2$d(HOpG_1*pG_2*)]·H_2O	52
D	CUHJIY	*cis*-[Pt(NH_3)$_2$(9-EtGua)$_2$]Cl_2·$3H_2O$	53
E	CUHJOE	*cis*-[Pt(NH_3)$_2$(9-EtGua)$_2$]$Cl_{1.5}(HCO_3)_{0.5}$·$1.5H_2O$	53
F	DEGXES	*cis*-[Pt(NH_3)$_2$(9-EtGua)$_2$]Pt$(CN)_4$·$3H_2O$	51
G	GUOAPT20	*cis*-[Pt(NH_3)$_2$(guanosine)$_2$]$(Cl)_{1.5}(ClO_4)_{0.5}$·$7H_2O$	54
H	SEWFAB	*cis*-[Pt(*n*-propylamine)$_2$(9-EtGua)$_2$]$(NO_3)_2$	55
I	BOHDAD	*cis*-[PtCl(NH_3)$_2$(2-Me,2-Me,9-MeGua)]PF_6	56
J	CYPTA10	*cis*-[Pt(NH_3)$_2$(1-MeCyt)(9-EtGua)]$(ClO_4)_2$	57
K	TGUOPT	[Pt(diethylenetriamine)(guanosine)]$(ClO_4)_2$	58
L	ENGUME	[Pt(trimethylenediamine)(guanosine-5′-monophosphate methyl ester)$_2$]·$11H_2O$	59
M	GEHGOP	[Pt(tmen)(9-MeGua)$_2$]$(PF_6)_2$·$2H_2O$	60
N	GEHGUV	[Pt(tmen)(9-EtGua)$_2$]$(ClO_4)_2$·$2H_2O$	60

[a] Cambridge Structural Database.[49] [b] This structure was refined with restraints. [c] This structure was refined without restraints. This species in a different space group (DETLIX20) was refined with loose restraints.[61]

We adopted Weiner's force field parameters for NB (bond stretching, angle bending and torsional, etc.) for NB1/NB2 of the guanine base when calculating the strain energies involving N7 within the guanine base. Similar adoptions of the AMBER force field for H3 hydrogens were also made (i.e. bond stretch, tetrahedral geometry of -[N31/N32]-[H3] of the AMBER -[N3][H3] were adopted). Only new force field parameters that are not provided in the AMBER force field in Discover 2.9 are discussed in this paper.

This new DNA/Pt force field was applied to several test systems to evaluate the validity of the parameters we introduced. For simple systems like $[Pt(NH_3)_3(9\text{-EtGua})]^{2+}$, point minimization procedures were used to minimize the structures to a delta rms gradient of 0.001 kcal/(mol·Å^2). For complex systems with many more conformational variables (e.g., *cis*-[Pt(NH_3)$_2$d(HOpG*pG*)]) a 500-ps dynamics simulation at constant temperature of 300 K was conducted and conformers were sampled every 1 ps. The collected structures (500 conformers for each dynamics simulation) were then minimized to a delta rms gradient of 0.001 kcal/(mol·Å^2). In all calculations, $\epsilon = 4r_{ij}$ was used and, in the typical way,[62] the 1−4 nonbond interaction term was scaled by a factor of 0.5.

Results and Discussion

Analysis of Crystal Structure Data. In previous studies, it has been shown that protonation of a six-membered ring nitrogen of purines or pyrimidines significantly expands the C−N−C interior angle.[63−65] Metal coordination has an effect about half as great.[65] However, Hodgson[66] has determined that metal ion coordination to N7 of the five-membered ring causes virtually no change. More crystallographic data have since become available, permitting a more extensive assessment of the effect of GN7 platination and protonation on the interior angles of G. Consistent with previous studies,[63,64] protonation of N7 of G results in small changes in the average interior angles of the five-membered ring (supplementary material, Table S1). These small changes are believable but statistically insignificant. Protonation caused relatively large (>3°) angle changes near the protonation site (∠C5−N7−C8 and ∠N7−C8−N9 expanded, ∠N7−C5−C4 reduced) and lesser (~2°) expansion of angles further away (∠C5−C4−N9 and ∠C4−N9−C8). The same trend, but with smaller changes, is seen with **platinated** compounds (supplementary material, Figure S1). Reported errors on the angles of the **platinated** data set for small

Table 2. New Atom Types and Force Constants

New Atom Types[a]

atom	description
PT	Platinum atom
NB1	N7 of guanine bound to Pt
NB2	N7 of the second Pt bound guanine; *cis* to the first
N31	Pt-bound ligand nitrogen, trans to NB1
N32	Pt-bound nitrogen of the second and/or the third non-DNA-base Pt ligands; trans to NB2 or another N32 and *cis* to NB1 and N31
H3	Proton bound to N31 or N32

Bond Stretch Deformation[a]

bond	r_0 (Å)	K_r (kcal/(mol·Å^2))
PT−NB1(NB2)	2.01	366
PT−N31(N32)	2.03	366

Angle Bend Deformation

angle	θ_0 (deg)	K_θ (kcal/(mol·rad^2))
CB−NB−CK [C5−N7−C8, Pt free][b]	104.1	70
CB−NB−CK [C5−N7−C8, N7 platinated][b]	104.1	70
CB−NB1(NB2)−PT [C5−N7−Pt][a]	127.95	20
CK−NB1(NB2)−PT [C5−N7−Pt][a]	127.95	20
NB1−PT−NB2 [N7(G1)−Pt−N7(G2)][c]	90	42
N31−PT−N32 [N(1)−Pt−N(2)][c]	90	42
N31−PT−NB2[c]	90	42
N32−PT−NB1[c]		
N31−PT−NB1[c]	180	42
N32−PT−NB2[c]		
N32−PT−N32[c]	180	42

Torsional Deformation[a]

torsional angle	ϕ_0 (deg)	n	V_n (kcal/mol)
CB−NB1−PT−N32	90	2	0.5
CK−NB1−PT−N32			
CB−NB2−PT−N31	90	2	0.5
CK−NB2−PT−N31			
CB−NB1−PT−NB2	90	2	0.5
CK−NB1−PT−NB2			
CB−NB2−PT−NB1			
CK−NB2−PT−NB1			

Improper Torsional Deformation[a]

improper angle	χ_0 (deg)	n	K_χ (kcal/mol)
CK−NB1−CB−PT	180	1	10
CK−NB2−CB−PT			

Nonbond Interaction

atom type	R (Å)[f]	ϵ* (kcal/mol)
PT[a]	4.88	0.4
NB1, NB2[d]	3.80	0.12
N31, N32[e]	3.70	0.08

[a] This work. [b] AMBER. [c] Kozelka, J.; Archer, S.; Petsko, G. A.; Lippard, S. J.; Quigley, G. J. *Biopolymers* **1987**, *26*, 1245. [d] The same as NB type of AMBER. [e] The same as N3 type of AMBER. [f] Diameters.

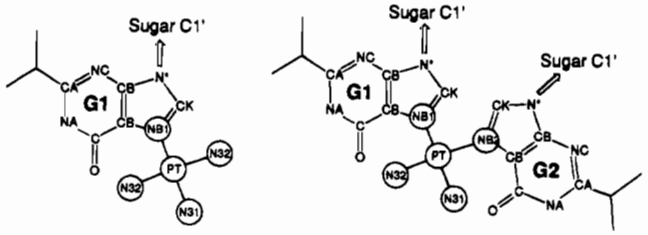

Figure 1. Newly introduced atom types for the new DNA/Pt force field (circled). All the other atom types are adopted from the original AMBER force field in Discover 2.9.

(62) *Discover User Guide, Part 1 (Version 2.9/3.1)*; Biosym Technologies: San Diego, CA, 1993.
(63) Ringertz, H. G. *The Purines-Theory and Experiment*; Israeli Academy of Sciences and Humanities: Jerusalem, 1972.
(64) Taylor, R.; Kennard, O. *J. Mol. Struct.* **1982**, *78*, 1.
(65) Nonella, M.; Hänggi, G.; Dubler, E. *THEOCHEM* **1993**, *98*, 173.
(66) Hodgson, D. J. *Prog. Inorg. Chem.* **1977**, *23*, 211.

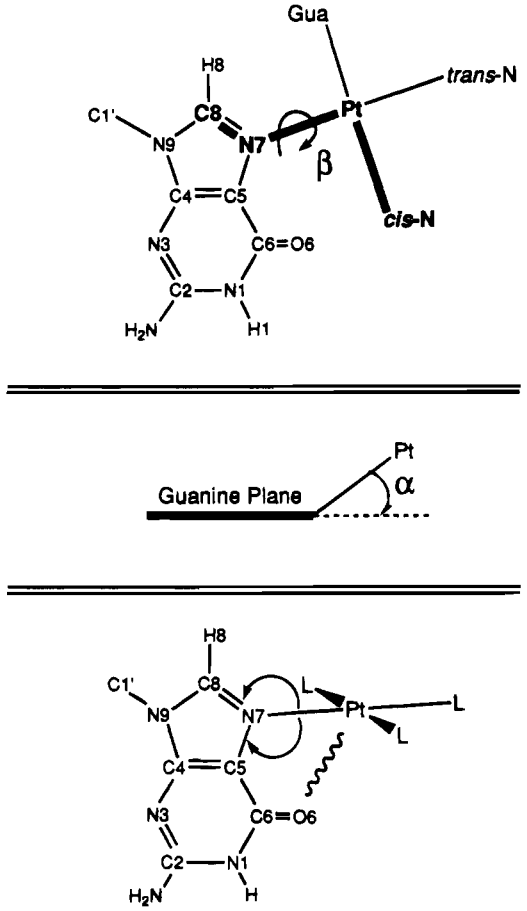

Figure 2. Definitions of important geoemtric parameters in G-adducts formed by Pt anticancer Drugs (cisplatin and its derivatives).

unrestrained structures were generally 1−2°.[51,53,54,57,60] Changes of only 0.54−1.37° of **platinated** from **free** G interior angles (supplementary material, Table S1) were calculated. Although it is reassuring that the changes induced by Pt, an electron-withdrawing group much less powerful than a proton, are smaller than but follow the same expansion/reduction pattern as the proton, the changes are not statistically significant.

Published crystal data show a wide range of possible relationships between the Pt coordination plane and the guanine base (for references, see Table 1). These relationships can be described by the β torsion angle (C8−N7−Pt−*cis*N), the α out-of-plane bending angle (angle formed by the Pt−N bond and the base plane), and the bond bending angles (∠C5−N7−Pt and ∠C8−N7−Pt) (Figure 2). The angles ∠C5−N7−Pt and ∠C8−N7−Pt can be treated together by analyzing their difference, Δ, the rocking angle. Crystal structure data show three populated ranges for β: a near perpendicular range and two skew forms, with the guanine six-membered ring rotated, in one toward the *cis*-amine ligand and in the other (less populated) toward the *cis*-guanine base (Figure 3). In different salts of the same cation, *cis*-$[Pt(NH_3)_2(9\text{-EtGua})_2]^{2+}$, there is a varied range of β torsion angles (i.e. β = 64.5° (F) to 84.1° (B) for the non-H-bonded 9-EtGua) (Figure 4).

The rocking angle (Δ = ∠C5−N7−Pt − ∠C8−N7−Pt) displays a range of −7° to +15° for *cis*-$[PtA_2G_2]$ structures, and the distribution is flat over the range (Figure 5). This rocking angle is positive in almost all cases, indicating that the ∠C5−N7−Pt angle is normally larger than ∠C8−N7−Pt. It is useful to note that Δ is positively correlated to the Pt−O6 through-space distance (Figure 6). As found for Δ, the Pt−O6 distance also shows a flat distribution (Figure 7), with the average at 3.49 Å (σ = 0.1 Å).

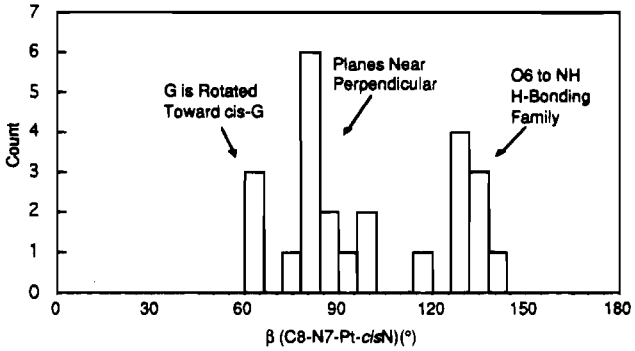

Figure 3. Histogram of β torsion angles form $[PtA_2G_2]$ crystal structures. $|\beta|$ was used for $\beta < 0$.

A previous analysis of structures of 6-oxopurine complexes[67] revealed a loose correlation between the β torsion angle and the Δ rocking angle. For conformations in which the guanine and platinum coordination planes are perpendicular ($\beta \approx 90°$), Δ was found to be small. When the guanine and platinum planes are closer to parallel ($\beta \approx 0°$ or 180°), steric interactions between O6 and the *cis*-ligand were found to cause the lopsided base to bend away, resulting in larger Δ values. This trend is confirmed by our analysis of a broader crystallographic data base (Figure 8).

Force Field Parameters. Bond Stretch. New parameters are needed for the two new bond types (PT−NB1/NB2 and PT−N31/N32), which we introduce into the DNA/Pt force field. Kozelka et al.[35] used a force constant of K_r = 201 kcal/(mol·Å^2) and a Pt−N bond length of 2.00 Å. Hambley,[38] on the other hand, used a force constant of K_r = 183 kcal/(mol·Å^2) and different bond lengths for Pt−N7 (2.01 Å) and Pt−N (2.03 Å). Because we believe that changes in angle bending and torsional angles are more variable than bond length deformations, we used stiffer Pt−N bond force constants with K_r = 183 or 366 kcal/(mol·Å^2) to maintain the Pt−N bond length close to the crystallographic distance (d_{N7-Pt} = 2.01 Å and $d_{N(ammine/amine)-Pt}$ = 2.03 Å). The results with either constant are virtually the same, although a value closer to the lower one may be prudent to use for larger systems such as duplexes. The lower value will allow all possible conformational transitions.

Angle Bend. The average interior angles from crystal data for **platinated** and **free** G's are not statistically different from equilibrium interior G angles in AMBER. Therefore, we adopted the AMBER values in the DNA/Pt force field. The only exception is that the ∠C8−N7−C4 value was adjusted from 103.8 to 104.1° so that the sum of the interior angles completes the 540° of a planar pentagon. This change is in the same direction caused by platination.

For the force constant of both ∠C5−N7−Pt and ∠C8−N7−Pt, Hambley[38] has used 21.6 kcal/(mol·rad^2) based on established values of Co(III) complexes, and Kozelka[35] has used 70 kcal/(mol·rad^2) based on values for *N*-alkylated purines. Our preliminary calculations indicated that Kozelka's larger force constants limited the range of Δ to low values. The analysis described above indicates that the rocking angle can have values from −7 to 15°; Δ is correlated with the C8−N7−Pt−*cis*-N torsion angle (β) and also depends on the nature of the amine ligand. Therefore, for C5−N7−Pt and C8−N7−Pt angle bending, we used a force constant of 20 kcal/(mol·rad^2). The equilibrium angle of 127.9° [$^1/_2$(360 − ∠C5−N7−C8)] was used for the two angles.

For the angles in the Pt(II) coordination plane, we adopted the right angle parameters of the *cis* ligand bonds and the coaxial

(67) Cavallo, L.; Cini, R.; Kobe, J.; Marzilli, L. G.; Natile, G. *J. Chem. Soc., Dalton Trans.* **1991**, 1867.

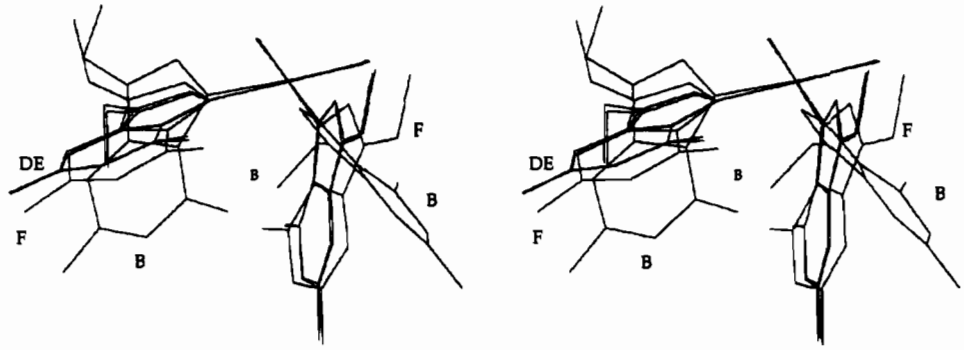

Figure 4. Stereoview of overlay of *cis*-$[Pt(NH_3)_2(9\text{-EtGua})_2]^{2+}$ cations each crystallized with different counterions (B, E, D, and F from Table 1). The Pt and ammine nitrogens were superimposed.

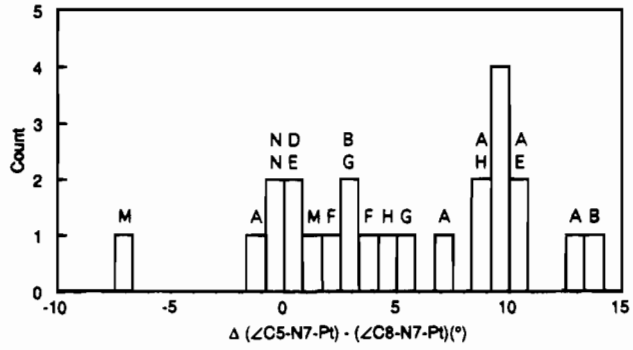

Figure 5. Histogram of Δ, the rocking angle from *cis*-$[PtA_2G_2]$ crystal structures. A positive value of Δ corresponds to a larger value of ∠C5–N7–Pt. Structure C was not included in this and later figures because of its size and method of refinement. It is one of the most accurate structures of its size, but the high quality of the data led the authors to report a structure refined without restraints.

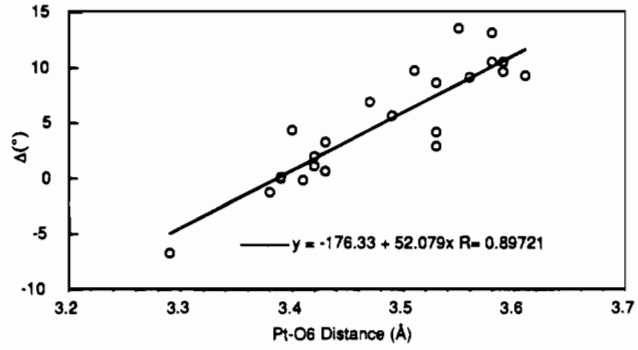

Figure 6. Correlation of Δ, the rocking angle, and the Pt–O6 through-space distance from *cis*-$[PtA_2G_2]$ crystal structures.

parameters of the *trans* bonds used by Kozelka et al.;[35] these were based on IR results,[68] Table 2.

Torsional Angle Deformation. A torsional energy term is normally essential for a molecular mechanics scheme based on van der Waals interactions.[69] The rotational potential around the Pt–N7 single bond is a critical parameter for the determination of the conformation of *cis*-PtA_2 DNA complexes. No experimental data are available yet to determine directly this rotational potential. However, the crystal structure data indicate that neither the O6–HN(ammine) bonding form nor the base plane–Pt coordination plane perpendicular form was clearly dominant (Figure 3). Therefore, we determined a suitable rotational parameter by adjusting the torsional force constant to a value which gives similar energy for the O6–HN(ammine)

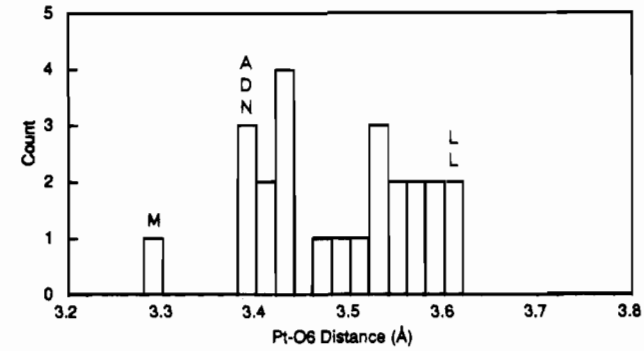

Figure 7. Histogram of Pt–O6 through-space distance from *cis*-$[PtA_2G_2]$ crystal structures.

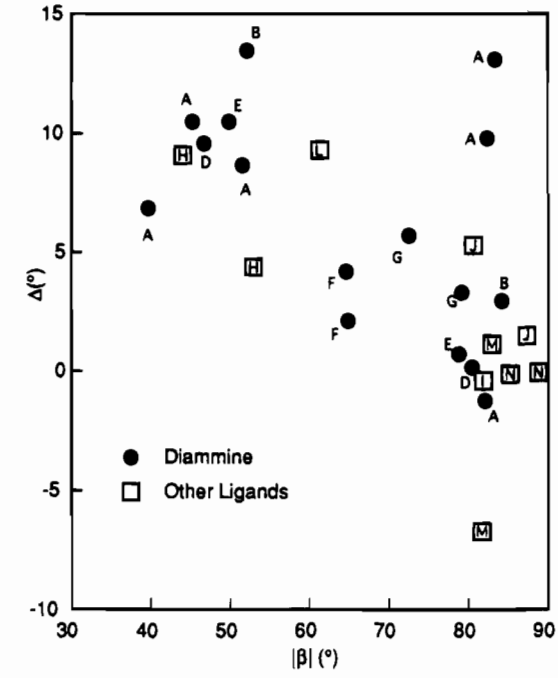

Figure 8. Absolute value of Δ vs β, the rocking angle. If $|\beta| < 90°$, $|\beta|$ is plotted, but when $|\beta| > 90°$, $180° - |\beta|$ is plotted. Labels correspond to Table 1.

hydrogen bonding and the base plane–Pt coordination plane perpendicular conformations of $[Pt(NH_3)_3(9\text{-EtGua})]^{2+}$ (see Figure 12, below). The torsional deformation force constant of 2.0 kcal/mol that was finally obtained was distributed equally over the four individual torsional angle terms around the N7–Pt bond (Table 2).

Out-of-Plane Deformation. The Pt–N7 bond bending out of the guanine plane (α, Figure 2) must be parametrized for the DNA/Pt force field. A large pucker of the coordinated

(68) Mizushima, S.; Nakagawa, I.; Schmelz, M. J.; Curran, C.; Quagliano, J. V. *Spectrochim. Acta* **1958**, *13*, 31.
(69) Burkert, U.; Allinger, N. L. *Molecular Mechanics*; American Chemical Society: Washington, DC, 1982.

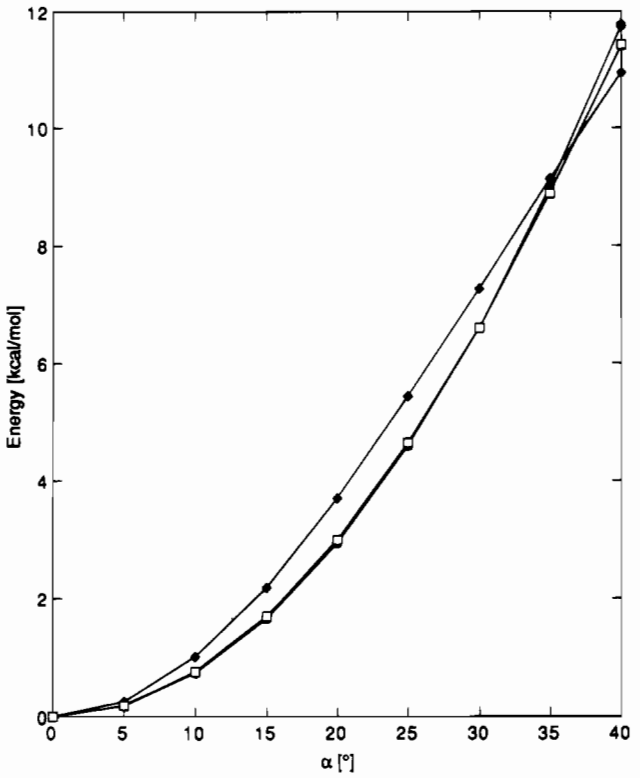

Figure 9. *Ab initio* energy after Kozelka et al.[70] for $[Pt(NH_3)_3(Ade)]^{2+}$ (− ● −), improper torsional energy from this work (− □ −), and the out-of-plane potential energy of Hambley (− ◆ −)[38] for *cis*-$[PtA_2Pu_2]$, as a function of the out-of-plane angle.

guanine ring results from using an improper torsional term (as defined in the AMBER force field eq 1) with a force constant of 6.7 kcal/mol on Pt−N7−X−X.[26] We evaluated two approaches to overcome this problem; both are based on the work of Kozelka and his colleagues.[26,70] One study recently reported *ab initio* calculations on the $[Pt(NH_3)_3(Ade)]^{2+}$ complex and gave the energy profile of the Pt−N7 out-of-adenine-plane bending.[70] We assume that $[Pt(NH_3)_3(Ade)]^{2+}$ and $[Pt(NH_3)_3$-(9-EtGua)$]^{2+}$ complexes have very similar out-of-plane parameters since both purines bind through N7. In one approach, we treated the out-of-plane potential with a single proper torsional function in the DNA/Pt force field. We based our energy vs improper torsional C8−N7−C5−Pt potential profile in eq 1 on Kozelka's energy vs out-of-plane angle profile. An improper barrier of 10 kcal/mol gave the best fit of the *ab initio* results (Figure 9). We used this value as the improper torsional force field constant. One Kozelka study also successfully used improper torsion angles to overcome the problem of guanine pucker.[26] However, the approach used four torsional angles, and the parameters were derived from previous calculations of a Pt pyrimidine compound. In a second approach, we used the more recent pseudo-bond-bending method suggested by Kozelka et al.[70] Both approaches gave basically the same and satisfying results in our test case of d(CTCCG*G*CCT)•(AGGCCGGAG)-*cis*-$Pt(NH_3)_2$ complex without significant base plane pucker (unpublished results, in preparation). The pseudo-bond-bending method is inconvenient because (i) an extra dummy atom in the center of the guanine five-membered ring must be defined, (ii) distance relationships between this dummy atom and each of the five ring-atoms must be provided, and (iii) a mass must be defined for the dummy atom in dynamics. Furthermore, extra forces among the five ring-atoms are inevitably introduced via this dummy atom and related constraints. Thus, we selected the single improper torsional approach parametrized here with a force constant of 10 kcal/mol for our DNA/Pt force field.

van der Waals Radius for Pt. Most metal−ligand coordination force fields do not include a van der Waals radius for the metal[40,71−73] because the metal usually is not accessible to 1−4 nonbonded interactions. However, the square planar geometry of platinum allows such an interaction, most notably with GO6. When the force constant for the ∠C5−N7−Pt and ∠C8−N7−Pt bending was small and Pt had no van der Waals radius, conformations with perpendicular G's (i.e., β's ~90°) yield large negative rocking angles (Δ) and much smaller Pt−GO6 distances than those observed crystallographically. Therefore, we performed calculations with different van der Waals diameter (R, diameter used in Biosym 2.9) and van der Waals depth (ϵ*) on $[Pt(NH)_3(9\text{-EtGua})]^{2+}$ to determine the best values. By using the parameters derived, R = 4.88 Å and ϵ* = 0.4 kcal/mol, and the original AMBER NB and N3 van der Waals parameters for NB1/NB2 and N31/N32, respectively, we were able to simulate the test crystals structures quite well (see below).

Hydrogen Bonding Parameters. Analysis of crystal structure data also indicated that O6−HN(ammine) H-bonds (N−O distances in the range of 2.91−2.97 Å) are similar in strength to those in DNA base pairs (N−O and N−N distances in the range of 2.82−2.95 Å).[74] The modified version of Weiner's AMBER force field H-bond parameters produce an average 10−12 H-bond energy (eq 1) of about −1.7 kcal/mol per H-bond for base pairs.[43] This 10−12 H-bond energy, together with the van der Waals and electrostatic contributions, gives a total of ~−3.4 kcal/mol per H-bond, which describes their "weak" characteristics. A normal H-bond has been calculated to have a binding energy in the neighborhood of −6 kcal/mol.[75−77] In Hambley's work,[38] the O6−HN(ammine) H-bond contributes as much as −4.5 kcal/mol per bond. This is smaller than the predicted normal single H-bonding energy (−6 kcal/mol) but still 1 kcal/mol more than the average H-bonding energy per H-bond in AMBER. Thus, the intramolecular O6−HN(ammine) H-bonding played a large role in determining the relative stability of the different *cis*-$[Pt(NH_3)_2(9\text{-EtGua})_2]^{2+}$ conformers in Hambley's work. We used the AMBER H2−O hydrogen bond parameters (A = 25686, B = 8106) for the O6−HN-(ammine/amine) H-bond. This parameter gives a maximum O6−H 10−12 energy per H-bond of about −1.7 kcal/mol at r_{OH} = 1.96 Å. The van der Waals and electrostatic contribution to this H-bond is as small as −0.5 kcal/mol.

Atomic Charges. There is still not a generally accepted set of atom charges for Pt−G complexes. In one approach, Kozelka et al. redistributed the 2+ charges only to the N7 and ammine nitrogen atoms and left +0.278 point charge on the Pt atom.[35] In another approach,[26] a population shift calculation for $[Pt(NH_3)_3(Gua)]^{2+}$ was used to obtain charges; if these charges were used instead of the AMBER charges, the negative point charges on both N7 and C5 atoms would have increased upon metal binding. We decided to develop a more realistic set of atom point charges for the DNA/Pt force field.

(70) Kozelka, J.; Savinelli, R.; Berthier, G.; Flament, J.-P.; Lavery, R. *J. Comput. Chem.* **1993**, *14*, 45.
(71) Drew, M. G. B.; Hollis, S.; Yates, P. C. *J. Chem. Soc., Dalton Trans.* **1985**, 1829.
(72) Niketic, S. R.; Rasmussen, K.; Woldbye, F.; Lifson, S. *Acta Chem. Scand.* **1976**, *A30*, 485.
(73) Niketic, S. R.; Rasmussen, K. *Acta Chem. Scand.* **1978**, *A32*, 391.
(74) Saenger, W. *Principles of Nucleic Acid Structure*; Springer-Verlag: New York, 1984.
(75) Bratoz, S. *Adv. Quantum Chem.* **1967**, *3*, 209.
(76) Lennard-Jones, J.; Pople, J. A. *Proc. R. Soc. London Ser. A* **1951**, *202*, 166.
(77) Pople, J. A. *Proc. R. Soc. London Ser. A* **1951**, *202*, 323.

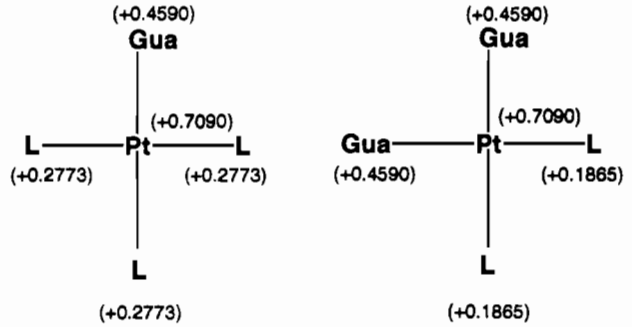

Figure 10. Gross distribution of the additional 2+ charge from Pt(II) to its ligands in two cases: (a) one coordinated G (b) two coordinated G's.

The atomic charges of the Pt-bound guanines were modified from typical AMBER values (see below) to account for the expected electron withdrawal from groups coordinated to the positively charged Pt(II). A similar charge transfer technique has been used by others in force field development.[78-80] The point charge on Pt was taken to be +0.709 based on *ab initio* potential charge fitting of $[Pt(NH_3)_3(Ade)]^{2+}$.[70] The net charge distributed to the purine (+0.459) was also taken from this study. This information was used to distribute charge onto the ligands starting with AMBER charges for guanine and CFF91 charges[79,80] for other ligands (amines/ammines). The gross distribution of the 2+ charge was as follows: +0.709 on the Pt, +0.459 to each coordinated guanine, and the remainder split between the other ligands (Figure 10). Distribution of the positive charge was based on proximity to the Pt; the ligand atoms were divided into three categories: primary (bound to Pt), secondary (bound to a primary atom), and tertiary (bound to a secondary atom). The net additional charge to each ligand was distributed between the atoms in a 10:3:1 ratio corresponding to their proximity to Pt (i.e. a primary atom received 10 times more additional charge than a tertiary atom). Table 3 lists the atomic charges for G and NH_3 ligands, and the charges for selected amine ligands and 9-Et and 9-Me groups are provided in the supplementary material (Table S2).

There is a need to see how sensitive the minimized conformation would be to the different charge sets. We compared the minimized structures of the HT and HH forms of *cis*-$[Pt(NH_3)_2(9\text{-EtGua})_2]^{2+}$ by using two different sets of atom point charges: the DNA/Pt set and the set of Herman et al.[26] The corresponding minimized conformers are superimposed in Figure 11. The low rms deviations for both the head-to-head (HH) and head-to-tail (HT) structures (Figure 11) of ~0.01 Å showed that the structures minimized with these two different sets of atom point charges were almost identical. Thus, in the DNA/Pt force field, the minimized conformation was not sensitive to the atom point charges used. However, we found that atom charges can alter the outcomes of the calculation if the assigned point charges are very different from those we used. For example, when a −0.600 point charge on GO6 was used in addition to the other charges of Herman et al., the O6−NH(ammine) electrostatic as well as the H-bond interactions became so dominant that the two O6−NH(ammine) H-bond conformer became the only local minimum. However, by using the force field parameters described above, the minimized conformations of $[PtA_xG_y]$ complexes should be similar using other reasonable atomic charge sets.

(78) Sun, H.; Mumby, S. J.; Maple, J. R.; Hagler, A. T. *J. Am. Chem. Soc.* **1994**, *116*, 2978.
(79) Maple, J.; Dinur, U.; Hagler, A. T. *Proc. Natl. Acad. Sci. U.S.A.* **1988**, *85*, 5350.
(80) Maple, J.; Thacher, T. S.; Dinur, U.; Hagler, A. T. *Chemical Design Automation News* **1990**, *5* (9), 5.

Table 3. Point Charge Distribution on $[PtA_xG_y]$ Complexes

atom	free base charge	platinated charge
	Guanine Base	
N1	−0.729	−0.729[a]
H1	0.336	0.336[a]
C2	0.871	0.871[a]
N2	−0.778	−0.778[a]
H21	0.325	0.325[a]
H22	0.339	0.339[a]
N3	−0.709	−0.709[a]
C4	0.391	0.414
C5	−0.060	0.009
C6	0.690	0.713
O6	−0.458	−0.458[a]
N7	−0.543	−0.314
C8	0.162	0.335
H8	0.150	0.069
N9	−0.042	−0.019
Pt		0.709
	Ammine Ligand[b]	
$PtG(NH_3)_3G]^{2+}$		
N		−0.600
H		0.293
cis-$[Pt(NH_3)_2G_2]^{2+}$		
N		−0.648
H		0.278

[a] Unchanged AMBER charge. [b] Amines and the 9-ethyl group in the supplementary material.

The DNA point charges as modified by Veal and Wilson[43] were adopted from the AMBER force field. This includes partially neutralized charges on phosphate groups so that the charge on each nucleotide is −0.2. Veal and Wilson use less neutralized phosphodiester charges in nucleotides which are part of an intercalation binding site for a cationic ligand (e.g. ethidium) to represent the release of counterions.[43] Similarly, for Pt(II)-bound nucleotides, we chose to use the original AMBER charges which are based on a full −1.0 charge per nucleotide for the 5′-phosphodiester atoms.

Molecular Mechanics Modeling Results. As our DNA/Pt force field was developed, we sought parameters that allowed us to obtain the best fit of the broad range of structures we were modeling. We should also point out that, when the crystal lattice forces were introduced by simulating the images in proper symmetry translations (periodic boundary conditions or PBC), generally even better fits between the energy minimized structures and the structures from crystal data are obtained (see below). This improvement suggests that the crystal packing environment plays a detectable role in determining the conformation of individual complexes in crystals. Some of the solid state structures are more relaxed, i.e. have lower strain energy, while some others are not so relaxed because of a greater effect from crystal packing forces. Molecular mechanics itself, without considering environmental effects, can only produce the most relaxed structure (which has the lowest strain energy corresponding to the force field) of a particular molecular species. It was essential that the force field developed be independent of any lattice effects. Below we describe how well our force field models known systems.

$[Pt(NH_3)_3(9\text{-EtGua})]^{2+}$. No structures are available with this cation. Two local minimia are found for $[Pt(NH_3)_3(9\text{-EtGua})]^{2+}$ under our force field. One has the base plane and the Pt coordination plane perpendicular to each other, and a second has a single O6-HN(ammine) hydrogen bond ($\beta \cong 120°$). The conformer with a single O6−HN(ammine) hydrogen bond is the global minimium. The torsional rotation barrier around Pt−N7 of this compound was calculated (Figure 12). The overall rotation barrier is about 9 kcal/mol under this force field. There is also a small barrier between the two low energy conformers.

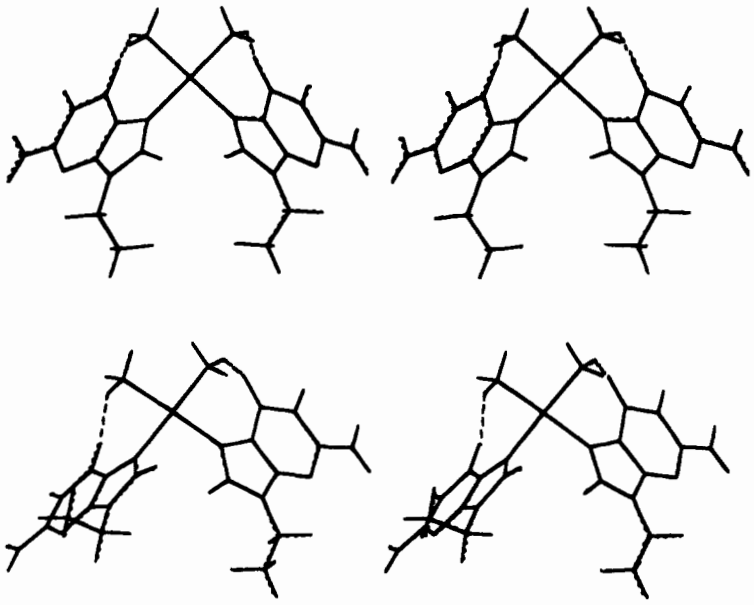

Figure 11. Stereoview of the structures of *cis*-$[Pt(NH_3)_2(9\text{-EtGua})_2]^{2+}$ complex with our atomic point charges (solid line) and with the Herman et al. charges[26] (dotted line) superimposed over all heavy atoms: Top, HH-2 conformer; bottom, HT-2 conformer.

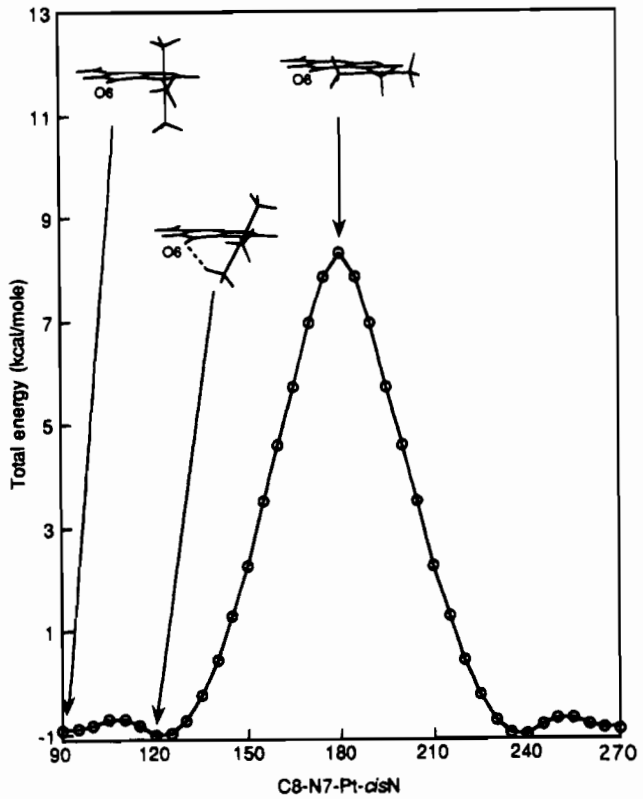

Figure 12. Rotation potential around the Pt−N7 bond of $[Pt(NH_3)_3(9\text{-EtGua})]^{2+}$. For clarity, the ethyl group is not shown.

The $E_{\text{hydrogen bond}}$ term (eq 1) contributes −1.6 kcal/mol to the total energy of the O6−HN(ammine) H-bonded conformer.

***cis*-[PtA$_2$G$_2$] Complexes (A = Ammine or Amine).** Six conformers of the *cis*-$[Pt(NH_3)_2(9\text{-EtGua})_2]^{2+}$ complex (Figure 13) corresponding to local minima were found: three head-to-head (HH) and three head-to-tail (HT) forms. In the HH conformer family, the most stable conformer had only one 9-EtGua O6−HN(ammine) H-bond. On the other hand, the HT conformers with one and two H-bonds lie 0.4 and 0.7 kcal/mol above the H-bond free HT conformer along the energy scale (Table 4). The DNA/Pt force field also predicted that the HT-0 conformer [the zero O6−HN(ammine) H-bond conformer] of *cis*-$[Pt(NH_3)_2(9\text{-EtGua})_2]^{2+}$ was energetically more favorable than any HH conformers. This is in agreement with solution NMR results on similar systems.[19] One important feature of the DNA/Pt force field is that, unlike the results obtained by Hambley,[38] it predicts that H-bond formation does not dominate the determination of relative stability of the *cis*-$[Pt(NH_3)_2(9\text{-EtGua})_2]^{2+}$ conformers.

In Figure 14a,b, the energy profile for a 360° rotation of one 9-EtGua in *cis*-$[Pt(NH_3)_2(9\text{-EtGua})_2]^{2+}$ is shown. There is an ~10 kcal/mol barrier for rotation around one Pt−N7 bond [C8−N7−Pt−*cis*-N torsional angle (β in Figure 2) changes from 90 to 180 to 270°] (Figure 14a). When the rotation is in this direction (bulky six-membered ring of G away from the *cis* G) the presence of the *cis* 9-EtGua base in *cis*-$[Pt(NH_3)_2(9\text{-EtGua})_2]^{2+}$ compared to the *cis* NH_3 in $[Pt(NH_3)_3(9\text{-EtGua})]^{2+}$ does not significantly increase the rotational barrier around the Pt−N7 single bond. The barrier is comparable to that in $[Pt(NH_3)_3(9\text{-EtGua})]^{2+}$ (Figure 12). Interestingly, the rotation barrier is about 2 kcal/mol higher when the C8−N7−Pt−*cis*-N torsional angle changes from 90 to 0 to 270° (bulky six-membered ring of G toward the *cis* G) (Figure 14b).

Next, several *cis*-$[PtA_2G_2]$ complexes in conformations similar to those in X-ray structures were energy minimized and superimposed on the X-ray determined structures using the guanine ring heavy atoms, the Pt atom, and the ammine/amine nitrogen atoms (Figures 15−17). The rms deviations (base ring heavy atoms, Pt atom, and ammine/amine nitrogen atoms) are given in captions. Three HH conformations of *cis*-$[Pt(NH_3)_2(9\text{-EtGua})_2]^{2+}$ (F, E, and B in Table 1) were simulated by this force field (Figure 15) with rms deviations ranging from 0.14 to 0.23 Å. Two HT species, *cis*-$[Pt(n\text{-propylamine})_2(9\text{-EtGua})_2]^{2+}$ (H in Table 1) and *cis*-$[Pt(NH_3)_2(\text{guanosine})_2]^{2+}$ (G in Table 1), were also modeled well by energy minimization (Figure 16).

The HT conformers in two crystal structures of a cation with the tmen (*N,N,N′,N′*-tetramethylethylenediamine) ligand, $[Pt(\text{tmen})(9\text{-MeGua})_2]^{2+}$ and $[Pt(\text{tmen})(9\text{-EtGua})_2]^{2+}$ (N and M in Table 1), were also reproduced by our force field (Figure 17). In this case, no H-bonding between the 9-EtGua and the amine ligand is possible. Our calculation indicated that the HT conformer of this complex was −1.64 kcal/mol more favorable than the HH conformer. A similar conclusion was also reached by Hambley for this H-bond free system.[38] The barrier to

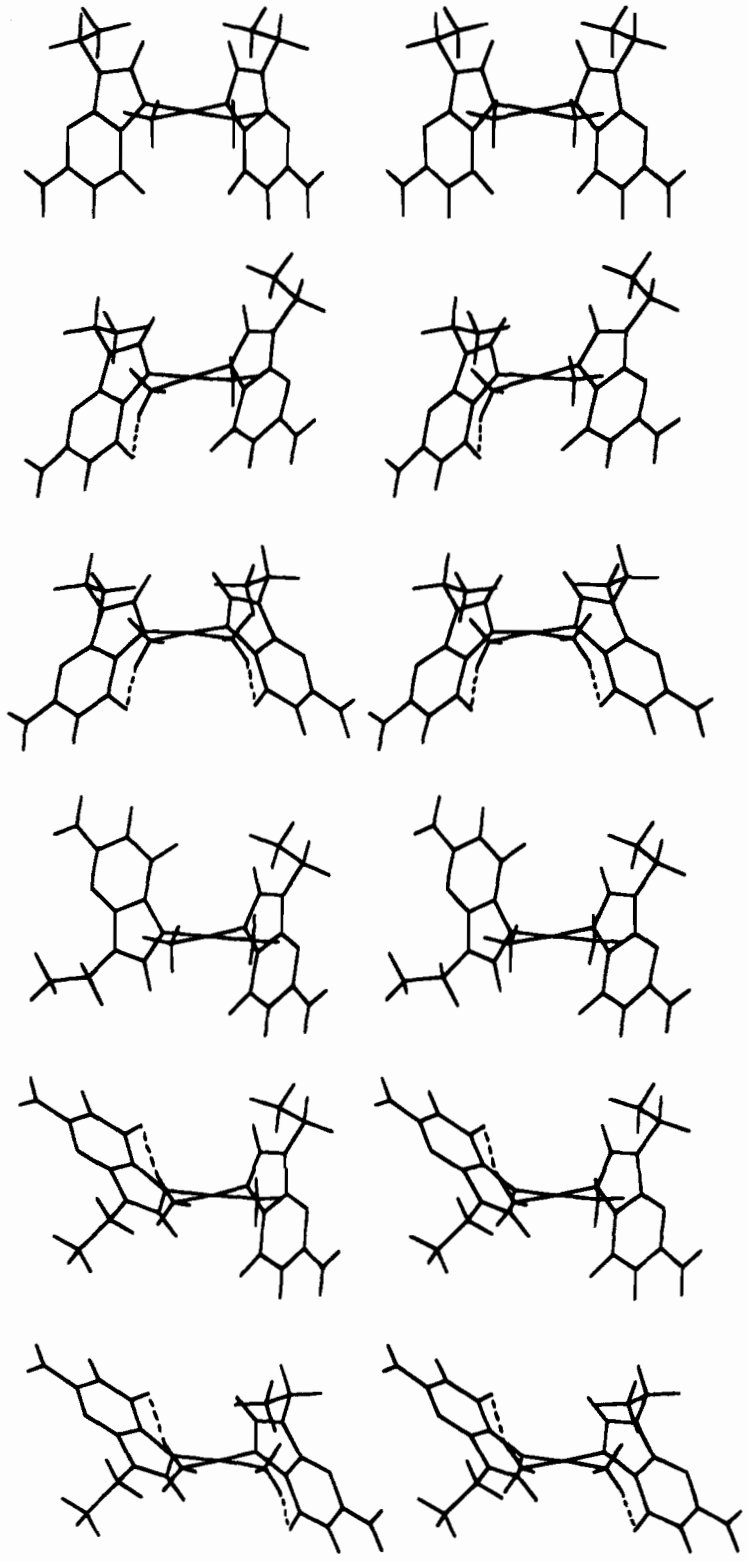

Figure 13. Stereopairs of the minimized structures of the *cis*-$[Pt(NH_3)_2(9\text{-EtGua})_2]^{2+}$ complex: Top to bottom, HH-0 (no H-bond), HH-1 (one H-bond), HH-2 (two H-bonds), HT-0 (no H-bond), HT-1 (one H-bond), and HT-2 (two H-bonds).

atropisomerization calculated by our force field was ~30 kcal/mol. This value is consistent with the NMR studies of Cramer and Dahlstrom,[81] who have estimated the lower limit of the $\Delta G^{\ddagger}$ for atropisomerization to be >21 kcal/mol. Hambley's force field calculated a barrier of 20 kcal/mol, i.e. slightly lower than the experimental lower limit.

***cis*-[Pt(NH$_3$)$_2$d(C$_1$pG$_2$*pG$_3$*)].** This structure (A in Table 1) is the largest species with a G*pG* intrastrand cross-link for which X-ray structures are available. It was refined using restraints. The unit cell of *cis*-[Pt(NH$_3$)$_2$d(C$_1$pG$_2$*pG$_3$*)] contains three distinct d(C$_1$pG$_2$*pG$_3$*) subunits (FEDFID 1−3). FEDFID 3 (which has the least packing interactions among the three) was compared to the energy-minimized structure (Figure 17). While the Pt(NH$_3$)$_2$(G base)$_2$ segments agreed well (rms deviation = 0.19 Å), somewhat larger deviations in the backbone segments were obtained. The biggest deviation between the minimized and crystal structures was found in the backbone

(81) Cramer, R. E.; Dahlstrom, P. L. *J. Am. Chem. Soc.* **1979**, *101*, 3679.

Table 4. Minimized Energy (kcal/mol) for *cis*-$[Pt(NH_3)_2(9\text{-EtGua})_2]^{2+}$ Complexes

	conformer		
H-bonds	HH	HT	HH−HT
0 H bonds	−13.65	−14.34	0.69
1 H bonds	−14.19	−13.89	−0.30
2 H bonds	−13.24	−13.66	−0.42

	conformer		
H-bonds	HH_{min}	HT_{min}	$HH_{min}-HT_{min}$
1 H bonds	−14.19		
0 H bonds		−14.34	−0.15

conformation of the C_1-G_2* junction. Energy minimization results in a conformation with all the backbone angles ($C_1\epsilon$ = −167.7, $C_1\zeta$ = −82.1, G_2*α = −73.0, G_2*β = −170.2, and G_2*γ = 56.4°) closer to the standard B-form values[74] than in the crystal structure ($C_1\epsilon$ = −125.0, $C_1\zeta$ = −69.0, G_2*α = −71.7, G_2*β = 172.7, and G_2*γ = 39.8). More interestingly, the crystal structure has only a weak O6−HN(ammine) H-bond (d_{N-O} = 3.0 Å). In the minimized structure, on the other hand, while the weak O6−HN(ammine) H-bond was maintained (d_{N-O} = 2.9 Å) a stronger phosphate O−HN(ammine) H-bond (d_{N-O} = 2.8 Å) was also formed. This type of phosphodiester phosphate O−HN(ammine) H-bond was frequently suggested by experimental results of solution systems[21,82,83] and by modeling computations.[26,34] A key finding in the solid state structure of *cis*-$[Pt(NH_3)_2d(HOpG_1$*pG_2*$)]$, the first cross-linked species successfully studied by X-ray methods, indicated that the 5′-psuedo phosphodiester group could form a H-bond.[84] This finding and the later indication of an albeit weaker H-bond to a phosphodiester group in *cis*-$[Pt(NH_3)_2d(C_1pG_2$*pG_3*$)]$ provided important information that buttressed our NMR evidence that such H-bonds were important in solution.[21]

Molecular Dynamics Modeling. For larger complexes, the single point energy minimization is usually not sufficient in searching low-energy conformers because of the substantially extended conformational space. Molecular dynamics (MD) simulation is a powerful tool to sample different conformers, which can then be used for single point energy minimization. We conducted a 500 ps constant-temperature (300 K) simulation and sampled 500 snapshots from the dynamics simulation trajectory. The structures from these 500 snapshots were then energy minimized.

***cis*-$[Pt(NH_3)_2d(C_1pG_2$*pG_3*$)]$.** The lowest energy conformation of *cis*-$[Pt(NH_3)_2d(C_1pG_2$*pG_3*$)]$ found in the 500 minimized MD snapshots is displayed in Figure 18. The majority of the 500 minimized structures were found to form a cytosine O2−HN(ammine) H-bond. The same NH_3 also formed a bifurcated H-bond with two O atoms of the P1 phosphate (C_1p). The other NH_3 formed a second H-bond with O6 of the *cis* G_3*. No G_2* O6−HN(ammine) H-bond existed in this low-energy conformation. Similar to the crystal structure, all low-energy conformations of this complex had the C3′-endo sugars for G_2* and C2′-endo sugars for G_3*. While the orientations of the C_1 residue relative to the rest of the complex are more or less the same in the MM and crystal structures, a quite different conformation is found in the MD structure. The C_1 residue is in an *anti* conformation in all three structures. However, the ζ angle of C_1 changes to 74° in the MD structure from −69° in the crystal structure. As a result, the entire C_1 residue has

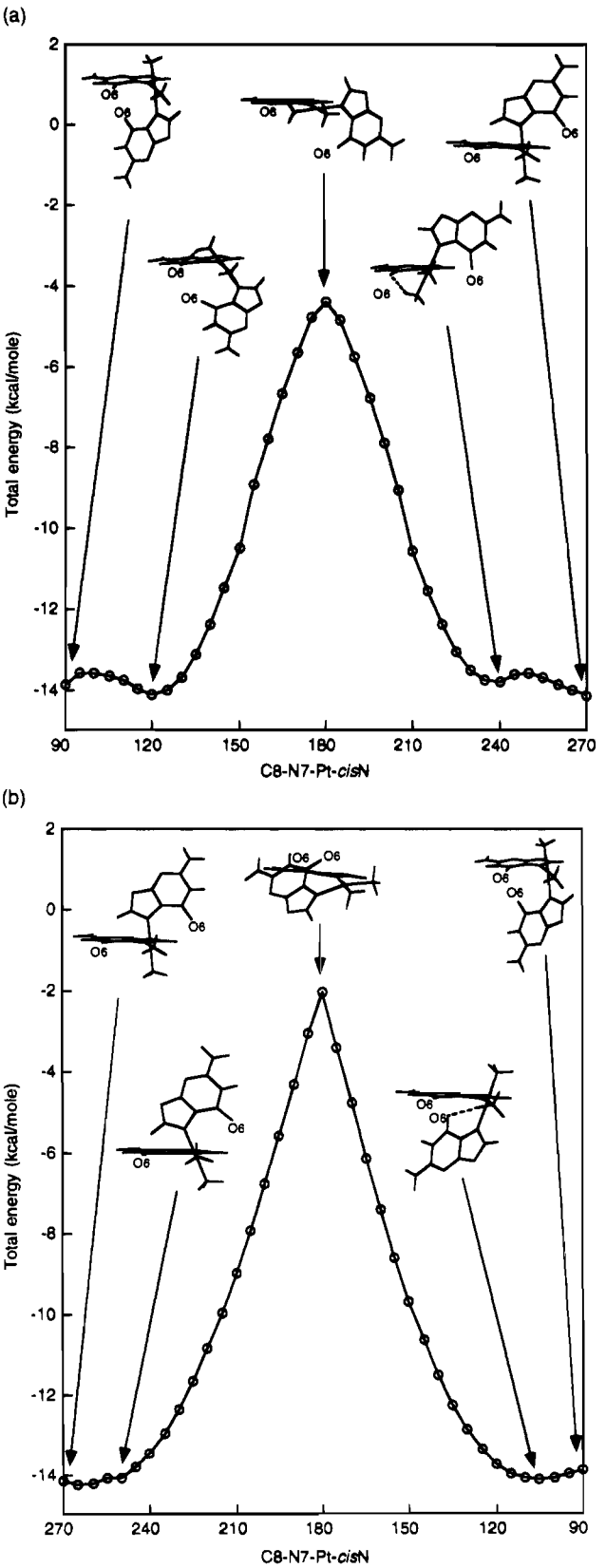

Figure 14. Rotation around one Pt−N7 bond for *cis*-$[Pt(NH_3)_2(9\text{-EtGua})_2]^{2+}$. The rotating 9-EtGua in the insets is shown in a horizontal position. The C8−N7−Pt−*cis*-N torsion angle of this 9-EtGua was fixed at the values shown on the abscissa. The remainder of the complex appears to rotate in respect to the horizontal "rotating" 9-EtGua with the *cis* ammine toward the top moving from the perpendicular orientation: (a) counterclockwise toward O6 and (b) clockwise away from O6. The six-membered rings move away from each other in (a) and toward each other in (b). For clarity, the ethyl groups are not shown.

(82) Bloemink, M. J.; Heetebrij, R. J.; Inagaki, K.; Kidani, Y.; Reedijk, J. *Inorg. Chem.* **1992**, *31*, 4656.
(83) Reedijk, J. *Inorg. Chim. Acta* **1992**, *198–200*, 873.
(84) Sherman, S. E.; Gibson, D.; Wang, A. H.-J.; Lippard, S. J. *Science (Washington D.C.)* **1985**, *230*, 412.

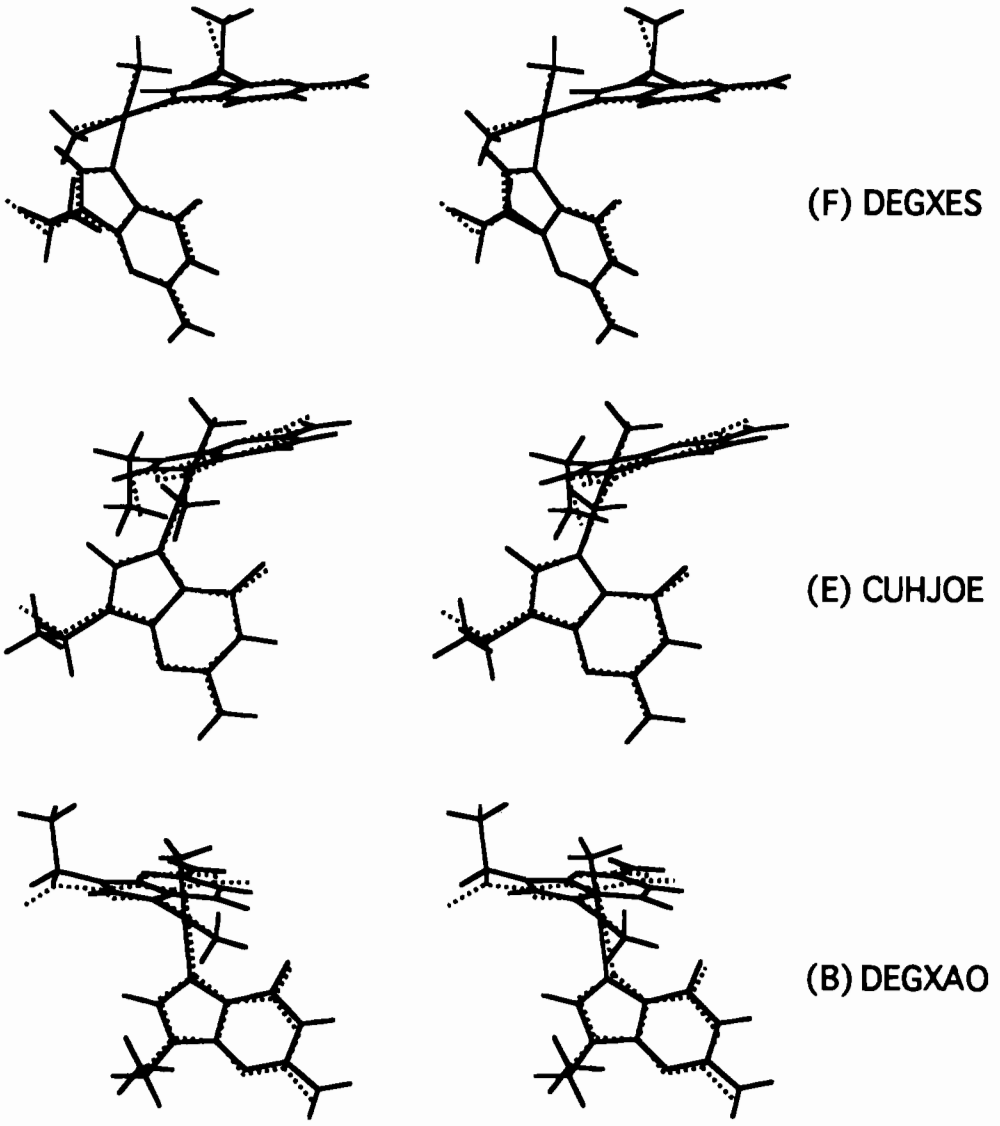

Figure 15. Stereoviews of three superimposed solid-state (dotted line) and the energy-minimized *cis*-$[Pt(NH_3)_2(9\text{-EtGua})_2]^{2+}$ HH structures. Only the guanine ring heavy atoms, the Pt, and the two coordinated N's of NH_3 were superimposed. Key: (F) DEGXES, rms deviation = 0.14 Å; (E) CUHJOE, rms deviation = 0.19 Å; (B) DEGXAO, rms deviation = 0.23 Å.

flipped. It remains on the top of G_2*, but in this orientation C_1 can now form an O2−H_3N H-bond. This reorientation is not surprising considering that the flexibility of the G*pG* segment is more restricted by the Pt cross-linking. The dynamics simulation allows the flexible terminal C residue to search more conformational space while the simple energy minimization MM procedure largely depends on the starting structure. The unique H-bond network found in this MD structure resulted in less agreement between the calculated and crystal structures (rms deviation = 0.5 Å for the heavy ring atoms of the two G's, the Pt and N of the NH_3 groups).

***cis*-[Pt(NH_3)$_2$d(HOpG$_1$*pG$_2$*)].** This is the second largest G*pG* species characterized by X-ray methods (C in Table 1). As mentioned above, the high quality of the data allowed the authors to perform unrestrained refinements. The 500 minimized structures of *cis*-[Pt(NH_3)$_2$d(HOpG$_1$*pG$_2$*)] exhibited two major classes of low-energy conformers, namely d(HOpG$_1$*pG$_2$*)-1 and d(HOpG$_1$*pG$_2$*)-2 (Figure 18). In both classes, G_1* and G_2* had C3′-endo and C2′-endo sugars, respectively. Comparison of the lowest energy conformers in each class shows d(HOpG$_1$*pG$_2$*)-1 had the lower total strain energy of −13.0 kcal/mol and d(HOpG$_1$*pG$_2$*)-2 had a slightly higher strain energy of −12.5 kcal/mol. In the d(HOpG$_1$*pG$_2$*)-1 conformer, one NH_3 formed a weak H-bond with G_2*O6. The HO−P1 group also formed an H-bond with the P2 phosphate (Figure 18). The backbone angles between the two residues are G_1*ϵ = −95.0, G_1*ζ = −65.0, G_2*α = 155.1, G_2*β = 175.7, and G_2*γ = 176.8°. In the d(HOpG$_1$*pG$_2$*)-2 conformer, both ammine groups formed a weak H-bond (d_{N-O} = ~2.9 Å) with the O6 of its *cis* G. One of the ammines also formed an H-bond with the P1 group (d_{N-O} = 2.8 Å). The backbone angles in this conformer are G_1*ϵ = −161.8, G_1*ζ = −62.8, G_2*α = 167.0, G_2*β = −177.4, and G_2*γ = −178.3°. In this particular system, it is interesting to note that the NH_3 *cis* to the 5′-side residue can interact simultaneously with O6 and the phosphate group of the 5′-G. Although the starting structure of this dynamics simulation has a B-form like backbone, both resulting low-energy structures have a trans−trans−trans conformation for $\alpha-\beta-\gamma$ of the G*pG* segment. This backbone conformation is also present in crystal structures[50,52] and has been found in previous calculations.[36] We have previously noted similarities in the conformation of the CG*G* segment in a 10-mer single strand and in the non-self-complementary duplex formed by the 10-mer.[85] This correlation suggests that the structure found in the crystals and by calculations may be relevant to duplex DNA.

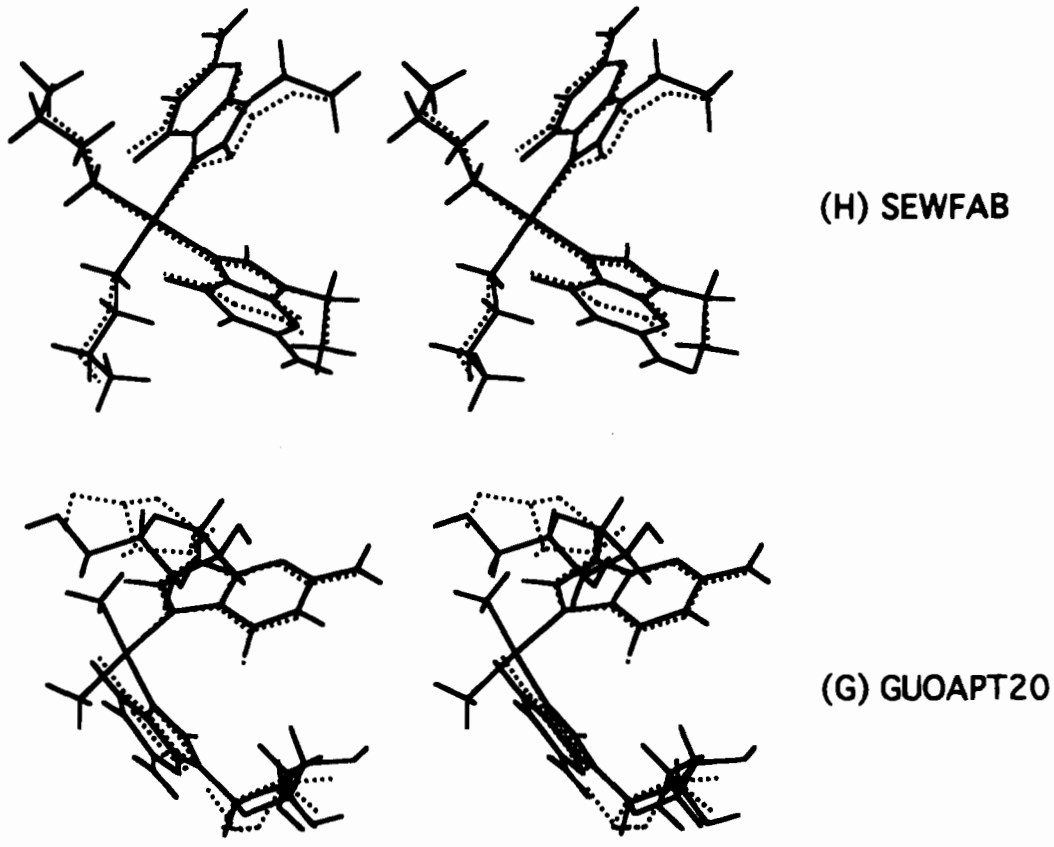

Figure 16. Stereoviews of two superimposed solid-state (dotted line) and the energy-miminized HT structures. Only the guanine ring heavy atoms, the Pt, and the two coordinated N's of A were superimposed. Two conformers: (top) *cis*-$[Pt(n\text{-propylamine})_2(9\text{-EtGua})_2]^{2+}$ (H) SEWFAB, rms deviation = 0.26 Å; (bottom) *cis*-$[Pt(NH_3)_2(guanosine)_2]^{2+}$ (G) GUOAPT20, rms deviation = 0.18 Å.

[$PtLG_2$]. As another test case, we evaluated the relative stability of the conformers of $[PtLG_2]$ [L = (*R,S,S,R-N,N'*-dimethyl-2,3-diaminobutane), G = 9-EtGua or 5′-GMPH (monoprotonated 5′-GMP)]. We wanted to compare the molecular mechanics results with our earlier NMR data.[20] For simplicity, we first studied the 9-EtGua complex with energy minimization methods. Two possible HT conformers exist for this compound; one has the potential of forming two O6-HN(amine) H-bonds (Λ form), and the other, none (Δ form) (Figure 19). Three local minima structures are found in the Λ conformer, with zero, one, and two O6−HN (amine) H-bonds, respectively. Lower strain energies were found for the conformers with multiple O6−HN H-bonds (Table 5). The HH conformer had only one local minimum with one O6−HN H-bond. This HH conformer had slightly higher strain energy than the two-H-bond ΛHT conformer (Table 5). The other HT conformer, ΔHT, was not energetically so favorable as the two-H-bond ΛHT conformer. The calculated ΛHT−HH conversion barrier was ≥13 kcal/mol. This is larger than the barrier calculated for both $[Pt(NH_3)_3(9\text{-EtGua})]^{2+}$ and *cis*-$[Pt(NH_3)_2(9\text{-EtGua})_2]^{2+}$ cases, as expected from the greater bulk of the *R,S,S,R-N,N'*-dimethyl-2,3-diaminobutane ligand compared to two *cis*-NH_3's.[20]

When G = 5′-GMPH, the complexity of the conformational search is greatly increased. We conducted 500-ps dynamics simulations at 300 K on $[PtL(5'\text{-GMPH})_2]$, starting with the HH and the ΛHT/ΔHT conformers. The ΛHT conformer has the potential of forming two O6−HN(amine) H-bonds (Figure 19). Its low-energy conformers can be categorized into two classes. The one (referred to as ΛHT-1 class) with the lowest strain energy has several H-bond interactions (Figure 20a). In this class of structures, O6 of the first G base forms an H-bond to the *cis* NH. The O6, H(N1), and H(N2) atoms of the second G base formed H-bonds with the phosphate group of the first 5′-GMPH (see ΛHT-1 in Figure 20a). The second class of low-energy ΛHT conformers (ΛHT-2, in Figure 20a) had a strain energy that was slightly higher than that of the ΛHT-1 class (Table 6). Both G bases formed an O6−HN H-bond with the *cis* NH, and the conformers had a pseudo C_2 local symmetry. The other HT atropisomer (ΔHT) does not have any O6−HN-(amine) H-bonding potential because of the stereochemistry of the *R,S,S,R-N,N'*-dimethyl-2,3-diaminobutane ligand. Three ΔHT structures with low strain energy are displayed in Figure 20b. The strain energies of all three ΔHT conformers were higher than those of the ΛHT atropisomers (Table 6). The ΔHT-0a and ΔHT-0b conformers also had internucleotide H-bonding interactions. Only ΔHT-0c had H-bonding interactions between the amine and the *cis* phosphate groups, but this ΔHT conformer had no internucleotide H-bonds. The lowest energy HH conformer of $[PtL(5'\text{-GMPH})_2]$ is also shown in Figure 20a.

NMR data on $[PtL(5'\text{-GMPH})_2]$ have suggested a O6−HN-(amine) H-bonding predominant structure, which is similar to the ΛHT-2 class in Figure 20a, as the stable solution conformation.[20] The NMR data also demonstrated an order of stability of ΛHT(major) ≫ HH > ΔHT(minor).[20] The calculations gave the stability order of ΛHT ≫ HH ~ ΔHT. Thus, our molecular mechanics calculations are in agreement with the experimental results. We also estimated the ΛHT to HH conversion barrier to be ≥18 kcal/mol, a barrier in agreement with the experimentally observed slow exchange behavior.

(85) Kline, T. P.; Marzilli, L. G.; Live, D.; Zon, G. *J. Am. Chem. Soc.* **1989**, *111*, 7057.

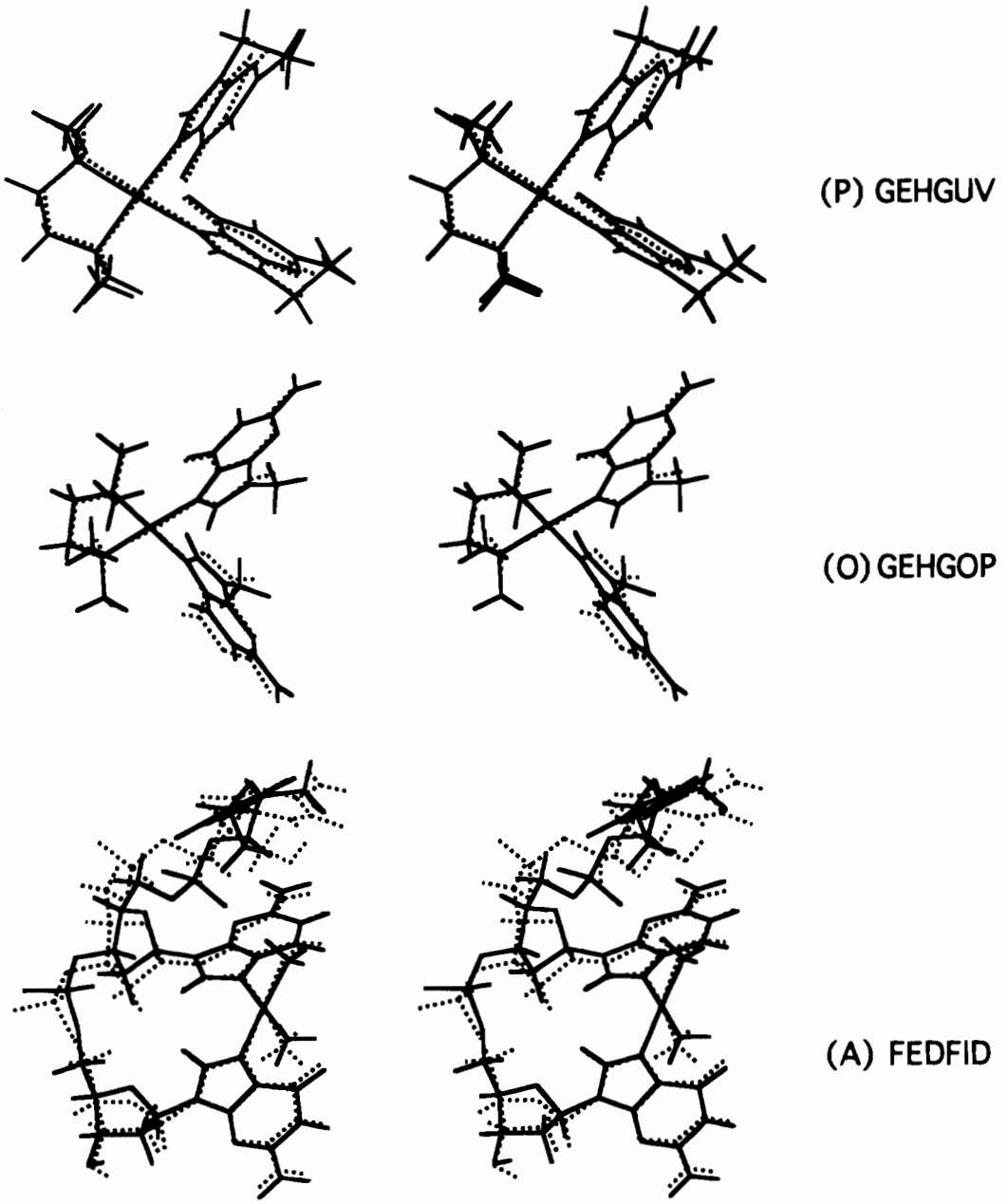

Figure 17. Stereoviews of the superimposed solid-state (dotted line) and the energy-minimized structures. Only the guanine base heavy atoms, the Pt, and the two coordinated N's of A were superimposed. Key: $[Pt(tmen)(9\text{-}EtGua)_2]^{2+}$ (N), GEHGUV, rms deviation = 0.18 Å; $[Pt(tmen)(9\text{-}MeGua)_2]^{2+}$ (M), GEHGOP, rms deviation = 0.22 Å; *cis*-$[Pt(NH_3)_2d(C_1pG_2{*}pG_3{*})]$ (A) FEDFID, rms deviation = 0.19 Å.

Crystal Packing Environment Effects. As mentioned above, a general force field should not depend on any crystal packing lattice and thus should be transferable from one system to another. When the crystal lattice effects are introduced, a successful force field should lead to calculated structures reflecting a particular crystal environment. In order to compare the minimized structures with the crystallographic ones, an attempt was made to simulate the crystal lattice environment using functions for periodic boundary conditions (PBC).[62] The minimizations were performed considering the effects of PBC and the presence of counterions and solvent. Four types of environment were simulated for each structure: a) no solvent/counterions and no PBC (gas phase), (b) no solvent/counterions and PBC (principal species array, PSA, only interactions between the Pt complexes in the lattice nearby), (c) solvent/counterions included and no PBC (unit cell), (d) solvent/counterions included and PBC (full lattice). This four-environment method independently tests the effects of explicit crystallographic solvent and counterions and the effects of the repeated lattice (PBC).

Cell dimensions, space groups, and initial heavy atom positions were taken from crystal coordinate files provided by the Cambridge Database. The PBC calculations employed the explicit image model,[62] where images of the interior molecules were generated according to symmetry operations and periodicity as far as 13 Å from the interior atoms. The interior molecules are affected by the nonbonded forces of their symmetrically related counterparts, whose positions are dictated by the positions of their corresponding interior atoms. Counterions and solvent molecules were restricted to their original crystallographic coordinates and were assigned approximate nonbonded parameters (supplementary material, Table S3). Water molecules were simulated with AMBER water atom types, and only the oxygen coordinates were fixed.

The minimized structures were compared to the original crystal coordinates by rms superimposition of heavy atoms

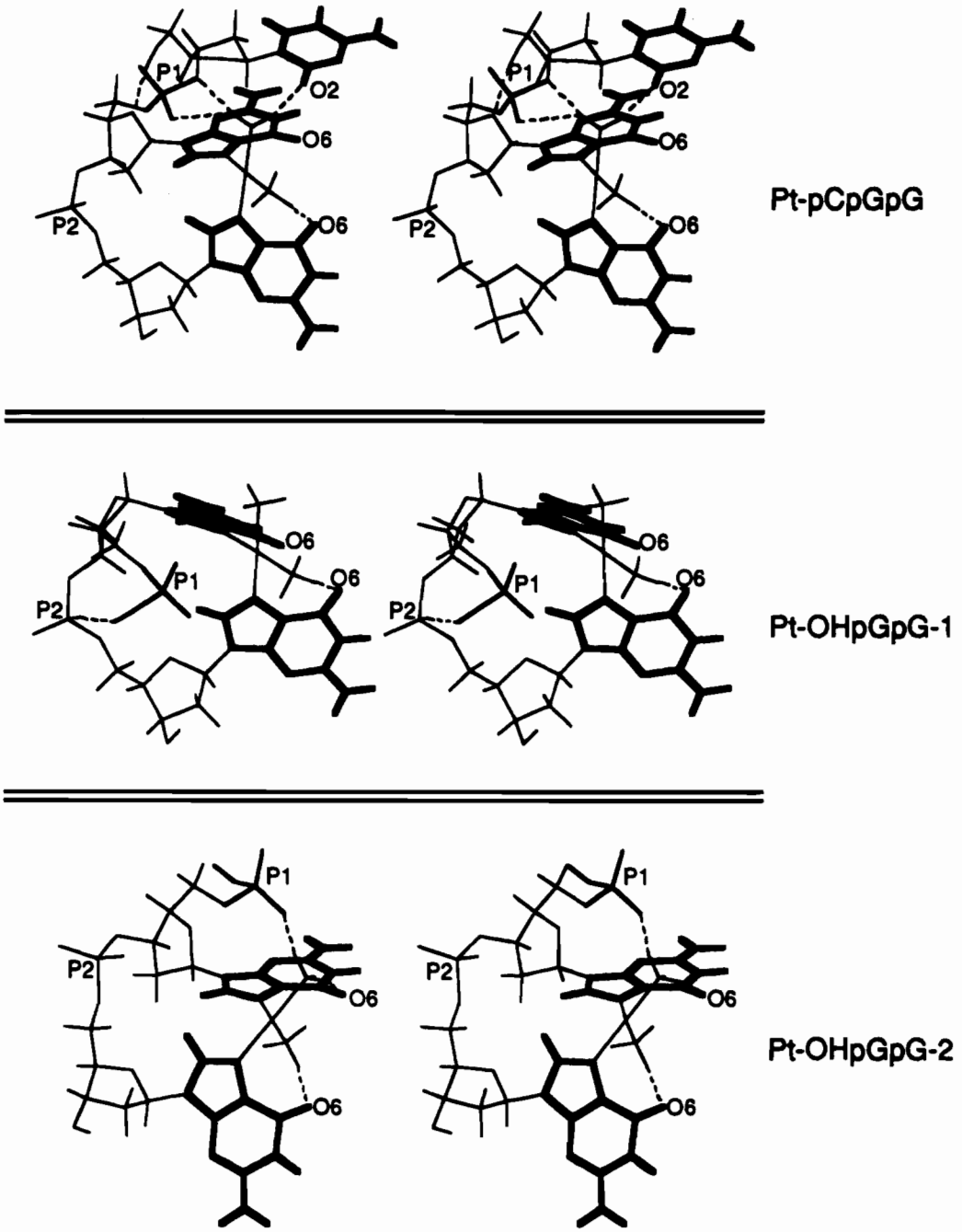

Figure 18. Conformers generated in a 500-ps MD simulation: Top, the lowest energy conformer of the *cis*-[Pt(NH_3)$_2$d(C_1pG_2*pG_3*)] complex; middle, d($HOpG_1$*pG_2*)-1; bottom, d($HOpG_1$*pG_2*)-2, the two low-energy conformers of *cis*-[Pt(NH_3)$_2$d($HOpG_1$*pG_2*)] complex.

(Table 7; supplementary material, Figures S2-S8). The rms deviation was calculated in two ways: (a) just with the guanine ring atoms, Pt, and ligand nitrogens; (b) with all heavy atoms in the crystal structure, except solvent and counterions. When the rms deviations of all the structures in Table 7 are averaged from each environment, the lowest average rms deviations come from the full lattice (0.09[a], 0.18[b]), the next the PSA (0.12[a], 0.21[b]), then gas phase (0.20[a], 0.32[b]), and finally the solitary unit cell (0.28[a], 0.46[b]). In nearly every case, the simulation with PBC yields structures closer to the crystal structure than those without PBC. The inclusion of crystallographic solvent and counterions when applying PBC slightly improved the fit (0.09[a] vs 0.12[a] and 0.18[b] vs 0.21[b]) but significantly worsened the fit in non-PBC minimizations (0.28[a] vs 0.20[a], 0.46[b] vs 0.32[b]).

The fact that calculations with simulated crystal lattice effects provided closer fits to the crystal structure from which they were modeled should come as no surprise. Nonbonded effects can exert strong effects, especially repulsive interactions due to the shape of the 6−12 potential. The improved fits with PBC support the method used to model lattice effects. In general, gas-phase minimizations fail to reproduce the full ranges of the β torsion angle (C8−N7−Pt−*cis*-N) (Figures 3 and 4) and Δ rocking angle (Figure 5) observed in the crystal structures. However, minimizations with the full lattice produce broader ranges of these two parameters which confirms that the force constants controlling the β torsion angle and Δ rocking angle are sufficiently weak to respond appropriately to crystal packing forces. This simulation suggests that the broad ranges of the β torsion angle and Δ rocking angle (Figures 3−5) seen experimentally is caused partially by lattice effects. Normal gas-phase minimization, which should not be expected to reproduce exactly the crystal structures, leads to structures with apparently high rms deviations compared to crystal structures (Figures 15−17).

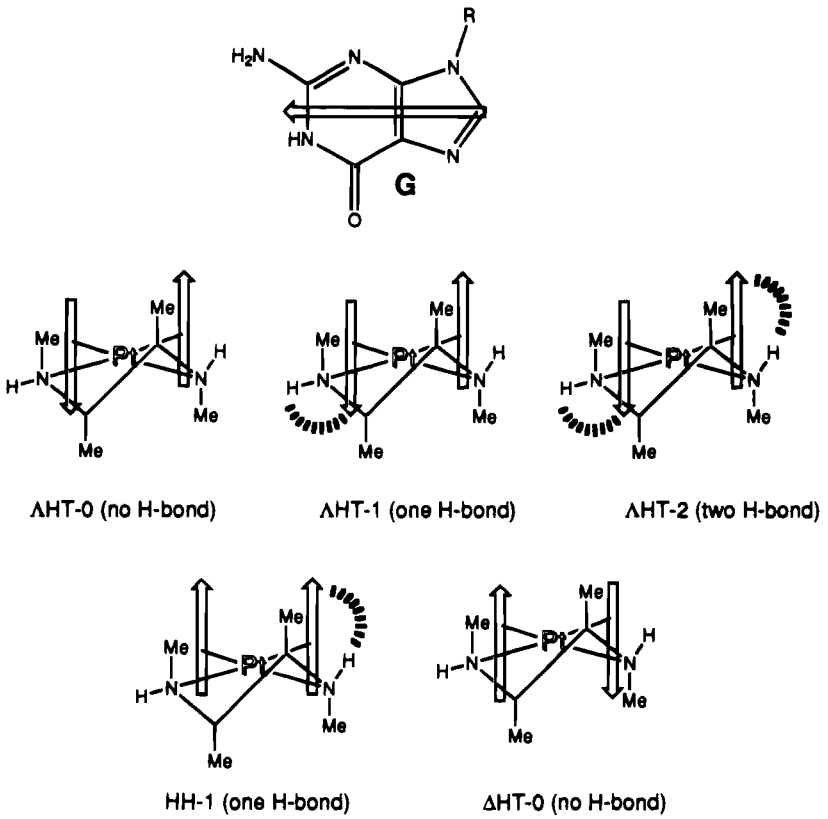

Figure 19. Scheme defining HH and HT orientation and Δ- and ΛHT conformers for [Pt(*R,S,S,R-N,N'*-dimethyl-2,3-diaminobutane)G_2].

Table 5. Minimized Energy (kcal/mol) for [Pt(*R,S,S,R-N,N'*-dimethyl-2,3-diaminobutane)(9-EtGua)$_2$]$^{2+}$ Complexes

conformer	energy (kcal/mol)	conformer	energy (kcal/mol)
ΛHT-1 (0 H-bond)	−5.09	HH-1 (1 H-bond)	−5.96
ΛHT-2 (1 H-bond)	−5.55	ΔHT-0 (0 H-bond)	−5.72
ΛHT-3 (2 H-bond)	−6.11		

Table 6. Minimized Energy (kcal/mol) for [Pt(*R,S,S,R-N,N'*-dimethyl-2,3-diaminobutane)(5'-GMPH)$_2$] Complexes

conformer	energy (kcal/mol)	conformer	energy (kcal/mol)
ΛHT-1	−22.5	ΔHT-0_b	−18.5[a]
ΛHT-2	−22.0	ΔHT-0_c	−17.8[a]
ΔHT-0_a	−20.5[a]	HH-0	−20.2

[a] The three ΔHT conformers have different base−phosphate interaction patterns.

Conclusions

After an analysis of many of the published solution and solid state studies of Pt complexes, we successfully constructed the necessary components for a molecular mechanics AMBER-type force field for modeling Pt complexes of guanine derivatives. The new parameters of the force field can be implemented within AMBER, which is widely available in many molecular modeling software packages. Molecular mechanics calculations on several test cases using this approach provided results that agree well with the available experimental data. A number of key force field parameters (i.e. Pt−N7−C angle bending, Pt−N rotation, Pt van der Waals parameters) were defined in this way. A satisfactory set of atomic charges for the *cis*-Pt site was constructed by redistributing part of the 2+ charge onto the atoms in the vicinity of Pt(II). The calculated conformation is not very sensitive to the atom point charges in the vicinity of Pt atom as long as a reasonable point charge set is selected. A van der Waals parameter for Pt is essential in this force field because of the square planar Pt coordination plane.

The DNA/Pt force field does not depend on any particular crystal packing environment, probably because a large crystal data base was used in its development. The application of this force field and the use of PBC to simulate crystal packing environments gave quite good agreement between the calculated structures and the corresponding crystal structures.

The calculations also gave reasonable agreement with atropisomer distributions and rotation barriers. The force field calculations predict that the sense of the guanine base rotation influences the barrier, and therefore rotation rates could reflect this preferential rotation direction. There is no evidence in the literature to our knowledge to support this prediction, but it seems reasonable. Another prediction is that the 5'-phosphate group could form H-bonds with the pyrimidine ring NH groups of the *cis* 5'-GMPH. Since there is no evidence for this type of interaction and since little difference has been found in the past between 3' and 5' nucleotide complexes with Pt(amines),[20] this prediction seems less reasonable but is testable. The phosphate−GN(1)H and −N(2)H interactions are most likely the result of the inadequacy of the solvent model.

Finally, we note that the primary motivation for this study was to evaluate further and to advance the use of molecular mechanics/molecular dynamics for defining structures of Pt anticancer adducts of DNA. Neither NMR nor X-ray methods are normally able to define very accurately the structure of the adducts. Furthermore, there is evidence that such adducts are highly fluxional and therefore need to be treated by molecular dynamics. An issue left unresolved in this study is whether the DNA/Pt force field, which clearly can account for features

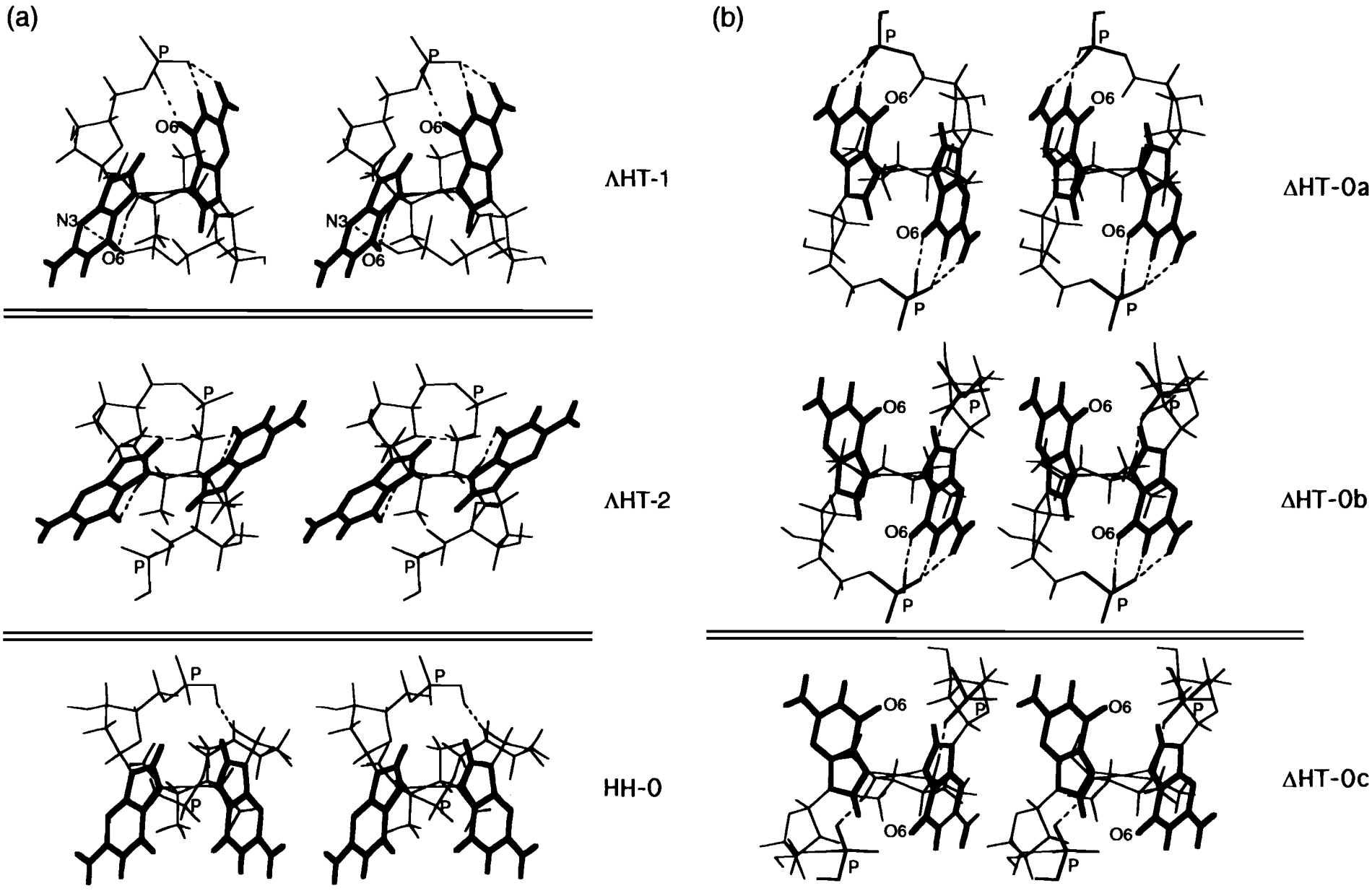

Figure 20. Low-energy conformers of [Pt(*R*,*S*,*S*,*R*-*N*,*N*′-dimethyl-2,3-diaminobutane)(5′-GMPH)$_2$] generated from a 500-ps MD simulation: (a) Top and middle, two low-energy ΛHT conformers with one and two O6-NH(amine) H-bonds and, bottom, the HH-0 conformer; (b) the three low-energy ΔHT-0 conformers.

Table 7. Statistical Analysis of Rms Deviations To Show Collective Differences between Environments

	no PBC[a]	PBC[a]	no PBC[b]	PBC[b]	no PBC -PBC[a]	no PBC -PBC[b]
	Solvent and Counterions Absent					
	gas phase	PSA	gas phase	PSA		
CUHJIY	0.21	0.10	0.28	0.16	0.11	0.12
CUHJOE	0.19	0.09	0.25	0.16	0.10	0.09
DEGXAO	0.23	0.07	0.40	0.17	0.16	0.23
DEGXES	0.14	0.15	0.38	0.23	−0.01	0.15
GEHGUV	0.18	0.16	0.31	0.32	0.02	−0.01
SEWFAB	0.26	0.12	0.32	0.21	0.14	0.11
avg	**0.20**	**0.12**	**0.32**	**0.21**	**0.09**	**0.12**
	Solvent and Counterions Included					
	unit cell	full lattice	unit cell	full lattice		
CUHJIY	0.22	0.08	0.53	0.14	0.14	0.39
CUHJOE	0.20	0.06	0.33	0.24	0.14	0.09
DEGXAO	0.18	0.07	0.37	0.09	0.11	0.28
DEGXES	0.45	0.14	0.60	0.18	0.31	0.42
GEHGUV	0.22	0.08	0.31	0.25	0.14	0.06
SEWFAB	0.41	0.13	0.63	0.19	0.28	0.44
avg	**0.28**	**0.09**	**0.46**	**0.18**	**0.19**	**0.28**

[a] The rms deviation was calculated by taking the ring atoms of guanine, Pt, and the N of the ammine/amine ligand(s). [b] The rms deviation was calculated by taking all the heavy atoms in the structure, not including solvent or counterions.

of small well-defined species, can also account for some unusual strain present in the adducts. Structures of longer nucleic acid *cis*-$Pt(NH_3)_2$ adducts are presently not known with sufficient accuracy, even though the *cis*-[$Pt(NH_3)_2d(HOpG_1*pG_2*)$][52] structure is one of the best determined structures of such size. It is an assumption of the molecular mechanics approach that a correctly defined force field will in the end allow calculation of local conformations that in turn determine global conformation. We continue to believe that a combination of experimental and computational methods will together provide the best insight into the nature of such adducts.

Acknowledgment. We wish to thank National Institutes of Health for financial support (Grant GM 29222), and we thank Professors Renzo Cini of the University of Siena, Stephen J. Lippard of MIT, and Suzanne Sherman of New College/USF for helpful comments.

Supplementary Material Available: Tables of average interior angles of five-membered rings from G crystal structures, charges on amine ligands and 9-Me/Et groups, charges and nonbonded parameters used for solvent and counterions in PBC calculations, and rms deviations for PBC calculations on *cis*-[$Pt(NH_3)_2d(C_1pG_2*pG_3*)$] and figures showing average interior angle changes of the guanine five-membered ring upon **protonation** and **platination** at N7 and structures calculated in various simulated lattice environments overlaid on the corresponding crystal structures (12 pages). Ordering information is given on any current masthead page.

IC940702N